Title	Cores and pH-dependent Dynamics of Ferredoxin-NADP+ Reductase Revealed by Hydrogen/Deuterium Exchange
Author(s)	Lee, Young-Ho; Tamura, Kosuke; Maeda, Masahiro; Hoshino, Masaru; Sakurai, Kazumasa; Takahashi, Satoshi; Ikegami, Takahisa; Hase, Toshiharu; Goto, Yuji
Citation	Journal of Biological Chemistry. 282(8) P.5959-P.5967
Issue Date	2007-02
Text Version	publisher
URL	http://hdl.handle.net/11094/71290
DOI	10.1074/jbc.M608417200
rights	
Note	

Osaka University Knowledge Archive : OUKA

https://ir.library.osaka-u.ac.jp/repo/ouka/all/

Osaka University

Cores and pH-dependent Dynamics of Ferredoxin-NADP$^+$ Reductase Revealed by Hydrogen/Deuterium Exchange*[s]

Young-Ho Lee[‡], **Kosuke Tamura**[‡], **Masahiro Maeda**[‡1], **Masaru Hoshino**[‡2], **Kazumasa Sakurai**[‡], **Satoshi Takahashi**[‡§], **Takahisa Ikegami**[‡], **Toshiharu Hase**[‡], and **Yuji Goto**[‡§3]

From the [‡]*Institute for Protein Research, Osaka University and* [§]*CREST, Japan Science and Technology Agency, 3-2 Yamadaoka, Suita, Osaka 565-0871, Japan*

NMR-detected hydrogen/deuterium (H/D) exchange of amide protons is a powerful way for investigating the residue-based conformational stability and dynamics of proteins in solution. Maize ferredoxin-NADP$^+$ reductase (FNR) is a relatively large protein with 314 amino acid residues, consisting of flavin adenine dinucleotide (FAD) and nicotinamide adenine dinucleotide phosphate (NADP$^+$)-binding domains. To address the structural stability and dynamics of FNR, H/D exchange of amide protons was performed using heteronuclear NMR at pD$_r$ values 8.0 and 6.0, physiologically relevant conditions mimicking inside of chloroplasts. At both pD$_r$ values, the exchange rate varied widely depending on the residues. The profiles of protected residues revealed that the highly protected regions matched well with the hydrophobic cores suggested from the crystal structure, and that the NADP$^+$-binding domain can be divided into two subdomains. The global stability of FNR obtained by H/D exchange with NMR was higher than that by chemical denaturation, indicating that H/D exchange is especially useful for analyzing the residue-based conformational stability of large proteins, for which global unfolding is mostly irreversible. Interestingly, more dynamic conformation of the C-terminal subdomain of the NADP$^+$-binding domain at pD$_r$ 8.0, the daytime pH in chloroplasts, than at pD$_r$ 6.0 is likely to be involved in the increased binding of NADP$^+$ for elevating the activity of FNR. In light of photosynthesis, the present study provides the first structure-based relationship of dynamics with function for the FNR-type family in solution.

Protein conformations as shown by x-ray crystallography or nuclear magnetic resonance spectroscopy are virtually dynamic entities over various time ranges in solution (1, 2). Clarifying such conformational motions at the level of the atom or residue is essential for understanding the structural stabilities of pro-

teins and the relationships between protein structures and functions (3–5). The hydrogen/deuterium (H/D)[4] exchange of amide protons in backbones has become an important way to address the motions of a protein from small or relatively large scale motions involved in biological functions such as binding of a substrate or releasing a product to much more large scale motions like a global unfolding process (4, 6). Among several approaches, the H/D exchange combined with heteronuclear NMR spectroscopy is the most convenient and powerful way because it can provide residue-specific information for most residues (7). For many globular proteins, this approach has identified protected cores, which are often composed of secondary structures buried inside the molecules and the cooperative interactions with partner molecules (4, 8), leading to allostery (9). Detailed analyses of exchanges in the native state of cytochrome c in the presence of various concentrations of denaturants suggested a pathway to unfolding, in which groups of secondary structural elements (*i.e.* foldons) are unfolded sequentially through distinct folding intermediates (10).

Although the impact of the H/D exchange method combined with NMR analyses is obvious, its application has been limited to proteins for which the amide resonances were already assigned. Therefore, the measurements have been performed with relatively small proteins, mostly less than 20,000 in a molecular weight (11). The largest proteins examined so far are bovine β-lactoglobulin (162 residues) (7), T4 lysozyme (164 residues) (12), and scFv (252 residues but with the same two domains) (13). Moreover, because the unfolding of proteins with a molecular weight greater than 20,000 is usually irreversible, a quantitative kinetic analysis of H/D exchange has not been established for large proteins.

Ferredoxin-NADP$^+$ reductase (FNR, 1.18.1.2) from maize leaf is a ubiquitous protein consisting of 314 amino acid residues. It catalyzes the transfer of electrons during photosynthesis: FNR receives two electrons from ferredoxin, a one-electron carrier protein, and transfers them to NADP$^+$ to produce NADPH (14). The activity and affinities for substrates of FNR decreased in response to a pH change from about 8 to 6 in chloroplasts (15). The three-dimensional structure of maize FNR composed of the well defined FAD- and NADP$^+$-binding domains has been solved by x-ray crystallography (16). The

---

[1] Current address: Laboratory of Biochemistry, Dept. of Chemistry, Graduate School of Science, Nagoya University, Chikusa-ku, Nagoya 464-8602, Japan.

[2] Current address: Graduate School of Pharmaceutical Sciences, Kyoto University, Yoshida-Shimoadachi 46-29, Sakyo-ku, Kyoto 606-8501, Japan.

[3] To whom correspondence should be addressed. Tel.: 81-6-6879-5614; Fax: 81-6-6879-8616; E-mail: ygoto@protein.osaka-u.ac.jp.

[4] The abbreviations used are: H/D, hydrogen/deuterium; FNR, ferredoxin-NADP$^+$ reductase; Fd, ferredoxin; C_m, midpoint concentration of unfolding; HSQC, heteronuclear single quantum coherence; pD$_r$, pH meter reading of D$_2$O solution; PF, protection factor.

FAD-binding domain (residues 1 to 153) is made up of a six-stranded antiparallel β-barrel the bottom of which is capped by an α-helix and a long loop. The NADP$^+$-binding domain (residues 154 to 314), a variant of the typical dinucleotide-binding fold (17, 18), consists of a central five-stranded parallel β-sheet surrounded by six α-helices. The FAD cofactor is tightly bound to the FAD-binding domain with its isoalloxazine ring sandwiched between the two domains, whereas the substrate NADP$^+$ binds to the NADP$^+$-binding domain. The binding of FAD is essential for maintaining the native structure, so that apo-FNR, lacking FAD, is assumed to have an intermediate conformation with a largely unfolded FAD-binding domain (19).

We have been studying the conformation and function of maize leaf FNR through heteronuclear NMR analyses with the recently achieved assignment for more than 95% of its amide protons (20). In the present study, taking advantage of the NMR assignment, we investigated the conformational stability of FNR using the H/D exchange of the amide protons. The results revealed the three protected core regions of FNR in which the NADP$^+$-binding domain can be divided into two subdomains with distinct differences in their motions. Moreover, the C-terminal subdomain exhibited a pH-dependent change of motions, implying a potential role in adjusting binding affinity of FNR for NADP$^+$ leading to effective functional control for photosynthesis in the daytime. Comparison of the apparent free energy change of unfolding (ΔG_{HX}) estimated for each residue on the basis of H/D exchange with the global free energy change of unfolding (ΔG_U) estimated from urea-induced unfolding suggests that H/D exchange provides a more reliable estimate of the stability of the core regions.

EXPERIMENTAL PROCEDURES

Sample Preparation—The *Escherichia coli* strain TG1 cells transformed with the plasmids containing the DNA of FNR were inoculated in 50 ml of a Luria-Bertani (LB) medium and grown overnight. This pre-cultured medium was added to 8 liters of a LB medium, and the bacteria were further incubated at 37 °C. The expression of the proteins was initiated by adding 1 mM isopropyl 1-thio-β-D-galactopyranoside when the cell density reached an absorbance of 0.65 at 600 nm. After additional incubation for 12 h, the cells were collected by centrifugation and disrupted by ultrasonication and the supernatant was applied to an anion-exchange column, DE52 (Whatman). The flow-through fraction was fractionated with ammonium sulfate at 40–70% saturation. The resulting precipitate was dissolved in 50 mM Tris-HCl buffer (pH 7.5) containing 40% ammonium sulfate, and the solution was loaded onto a gel-filtration column of Sephadex G-25 (Amersham Biosciences), pre-equilibrated with a 50 mM Tris-HCl buffer (pH 7.5). Unless otherwise noted, all chromatographic columns were equilibrated with 50 mM Tris-HCl buffer (pH 7.5). The FNR fraction was further separated by anion exchange chromatography with DEAE-Toyopearl (Tosoh, Japan). FNR was eluted by applying a linear gradient of the NaCl concentration from 0 to 0.5 M in the same buffer, monitored by measuring absorbance at 280 nm in the ÄKTA system (Amersham Biosciences). In the last purification step, an affinity chromatography of a Fd matrix was used

as described previously (19, 20). The purity of FNR was confirmed by SDS-polyacrylamide gel electrophoresis. The protein concentration was determined by absorption using extinction coefficients of 10,000 M^{-1} cm^{-1} at 460 nm and 47,800 M^{-1} cm^{-1} at 280 nm.

To obtain a uniformly ^{15}N-labeled FNR for NMR measurements, a colony of the transformed cells was grown in 50 ml of LB medium containing 0.14 mM ampicillin at 37 °C for 6 h, and then 10 ml of the medium was inoculated with 1.5 liters of an M9 minimum medium containing 1.24 g/liters of (^{15}NH$_4$)$_2$SO$_4$ as a sole nitrogen source. The procedure used to purify ^{15}N-labeled FNR was identical to that used for non-labeled FNR.

CD and Fluorescence Measurements—CD measurements were carried out in a J-720WI spectropolarimeter (Jasco, Japan) using a cell with a 1-mm light path at a protein concentration of 4 μM. The results were expressed as the mean residue ellipticity, $[\theta]$, defined as $[\theta] = 100\ \theta_{obs}/l\ c$, where θ_{obs} is the observed ellipticity in degrees, c is the concentration in residue moles/liter, and l is the length of the light path in cm. The temperature was controlled by a Jasco PTC-348WI peltier system. Fluorescence emission spectra were recorded at 25 and 40 °C in a 25 mM sodium phosphate buffer (pH 8.0), using an F-4500 fluorometer (Hitachi, Japan) and at 40 °C in the same buffer (pH 6.0) in the presence and absence of 50 mM NaClO$_4$. For the fluorescence spectrum of FAD, it was excited at a wavelength of 453 nm. The protein concentration was set at 1 μM, and the temperature was maintained by a thermostatically controlled water bath. Equilibrium denaturation experiments were done as follows. Protein solutions containing various concentrations of urea were preincubated for at least 24 h at room temperature prior to the experiments. The transitions were followed by measuring the far UV CD and fluorescence intensity of FAD. For CD measurements, the change in ellipticity at 222 nm was recorded. Relative fluorescence intensity was recorded at 530 nm with an excitation wavelength at 453 nm.

The resulting transition curves were analyzed by non-linear least squares curve fitting assuming a two-state transition (21) as shown in the following equation.

$$[\text{Signal}] = \frac{(a + b[\text{D}]) + (c + d[\text{D}])\exp\left(\dfrac{m([\text{D}] - C_m)}{RT}\right)}{1 + \exp\left(\dfrac{m([\text{D}] - C_m)}{RT}\right)} \quad \text{(Eq. 1)}$$

In Equation 1, [Signal] is either the ellipticity at 222 nm or fluorescence at 530 nm, a and c are the intercepts, b and d are the slopes of the base lines for native and unfolded species, and [D] and C_m are the concentration of urea for each experiment and the concentration at the midpoint of the reaction, respectively. For the transition curves at pH 8.0 and 25 °C, when reliable pre- and post-transition base lines could not be obtained because of a scarcity of data points, the base lines in accordance with other base lines were defined manually (see Fig. 1).

NMR Measurements—NMR spectra were measured at 40 °C on a Bruker DRX-800 spectrometer equipped with a cryogenic triple-resonance probe or a DRX-600 equipped with a triple axis-gradient triple resonance probe. Two-dimensional heteronuclear single quantum correlation (HSQC) spectra were

recorded with a spectral width of 12,820.5 Hz (1,024 complex points) for ^{1}H and 2,439.0 Hz (128 complex points) for ^{15}N dimensions with four or eight scans accumulated for each free induction decay for 1.3 h. The field frequency was locked at the deuterium signal from D$_2$O. Spectra were processed using nmrPipe (22) and analyzed with nmrDraw, PIPP, and Sparky.

H/D exchange was performed in the presence and absence of 2 M urea at 40 °C and pD$_r$ 8.0, and in the absence of urea at 40 °C and pD$_r$ 6.0. Exchange was initiated by manually mixing lyophilized FNR with a 25 mM d-sodium phosphate buffer at pD$_r$ 8.0. In the case of measurements at pD$_r$ 6.0, a dilution method was applied where 30 μl of a 5 mM FNR solution dissolved in a 25 mM sodium phosphate buffer containing 50 mM sodium perchlorate at pH 6.4 was mixed with 270 μl of the same concentration of deuterium buffer at pD$_r$ 6.0. Unless otherwise stated, all NMR measurements were carried out at 40 °C and, for the measurements at pD$_r$ 6.0, 50 mM NaClO$_4$ was added. The amide proton decays were monitored by measuring peak intensities in a series of two-dimensional ^{1}H-^{15}N HSQC spectra. The decay curves were fitted to a single exponential curve to obtain the apparent rate constant of exchange (k_{app}). The intrinsic rate constant (k_{int}) values were calculated with the SPHERE program (23).

RESULTS

Global Unfolding of FNR Induced by Urea—We characterized the global stability of FNR by measuring urea-induced unfolding under several conditions. First, the apparent unfolding transitions induced by 1 day of incubation at 25 and 40 °C at pH 8.0 in the presence of various concentrations of urea were measured with far UV CD and fluorescence of FAD (Fig. 1A). The far UV CD of FNR in its native state exhibited a spectrum typical of α/β proteins (data not shown; see Ref. 19) in accord with the x-ray crystallographic structure. The addition of high concentrations of urea resulted in global unfolding, providing a CD spectrum of a random coil state. The transition curves constructed from ellipticity at 222 nm were cooperative with apparent C_m values of 5.9 M at 20 °C and 3.9 M at 40 °C, showing that the increase of temperature destabilized FNR (Fig. 1A and supplemental Table S1). In the native state, the fluorescence of FAD is completely quenched (19). The urea-induced unfolding led to the release of FAD, producing a strong fluorescence of free FAD with a maximum at 530 nm. The transition curve after incubation for 1 day monitored by measuring the fluorescence of FAD coincided with that monitored using CD (Fig. 1A). This suggests that urea-induced unfolding is a cooperative process in which unfolding of the secondary structure and the release of FAD occur concomitantly.

As expected for large proteins, the unfolding of FNR, made up of 314 amino acid residues and the cofactor FAD, was not reversible (19): the refolding yield after unfolding in a high concentration of urea (*e.g.* 8 M) was 10–30% depending on the methods and conditions used. Irreversible unfolding will lead the apparent transition curve to be dependent on the incubation time. With an increase in the period of incubation in urea, the concentration of urea required for unfolding decreased when the unfolding was monitored by the fluorescence of FAD (Fig. 1B). We also measured the unfolding transitions at pH 6.0
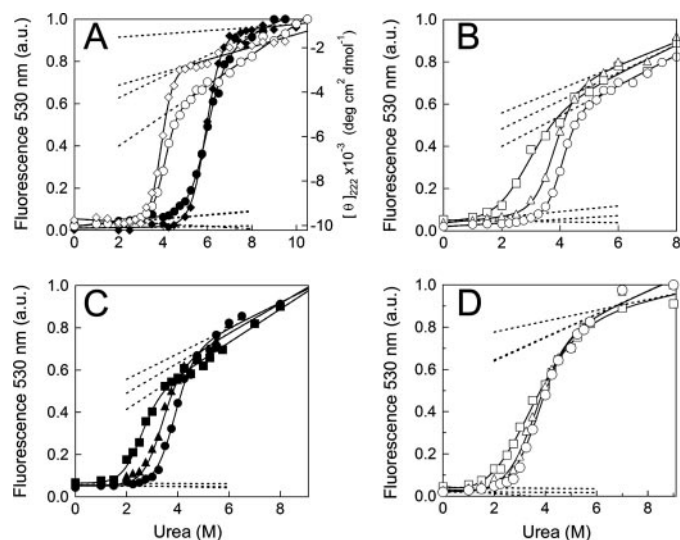

FIGURE 1. **Urea-induced unfolding transitions of FNR.** *A*, unfolding curves were constructed from the ellipticity at 222 nm ($\Diamond$, $\blacklozenge$) and fluorescence of FAD at 530 nm ($\bigcirc$, $\bullet$) after incubation for 1 day at pH 8.0 and 25 (*closed symbols*) or 40 °C (*open symbols*). *B–D*, dependence of the unfolding transition curves on the incubation time observed with fluorescence at pH 8.0 (*B*) and pH 6.0 in the presence (*C*) and absence (*D*) of 50 mM NaClO$_4$. The incubation times were 1 ($\bigcirc$, $\bullet$), 3 ($\triangle$, $\blacktriangle$), and 7 ($\blacksquare$, $\square$) days. All experiments were carried out at 40 °C. The *solid lines* indicate the transition curves fitted assuming a two-state mechanism and the *broken lines* represent the base lines derived from the fittings. Details are provided under "Experimental Procedures."

and 40 °C, where the catalytic activity of FNR is suppressed (15), exhibiting the same effects of incubation time on the apparent stability (Fig. 1D). The apparent transition curves showed that the stability is greater at pH 8.0 than at pH 6.0. In this research, to increase the solubility of FNR required for the NMR measurements, we added 50 mM sodium perchlorate (NaClO$_4$) to the FNR solution at pH 6.0. Because NaClO$_4$ is a chaotropic salt known to denature proteins at high salt concentrations (24), the unfolding in the presence of 50 mM NaClO$_4$ (Fig. 1C) was also measured with the same incubation periods as in its absence. The results indicated that the apparent stability is slightly increased by a low concentration of NaClO$_4$ as used in the present study. Although this might represent specific effects of the salt, the effects were too small to be addressed in this study.

Although the unfolding transitions of FNR were not reversible, we provisionally analyzed the transition curves on the basis of an equilibrium two-state mechanism. Consequently, the apparent parameters were obtained, including the free energy change of unfolding (ΔG_U) in the absence of denaturant (supplemental Table S1).

H/D Exchange Monitored by NMR—The two-dimensional ^{15}N-^{1}H HSQC spectrum exhibited more than 314 amide group cross-peaks (Fig. 2A), of which 285 were assigned, accounting for ~95% assignments (excluding the N terminus and 13 Pro residues) (20). With these cross-peaks, we previously detected the protected amide protons by performing a H/D exchange for 3 days (20). Here, we carried out a far more detailed analysis of the H/D exchange kinetics, first, at pD$_r$ 8.0 and 40 °C, where pD$_r$ is a pH meter reading of the D$_2$O solution. The H/D exchange was initiated by dissolving the lyophilized FNR sample into the pD$_r$ 8.0 buffer. At the shortest sampling time of 40 min (*i.e.* dead time), which included the time for preparing the NMR sample
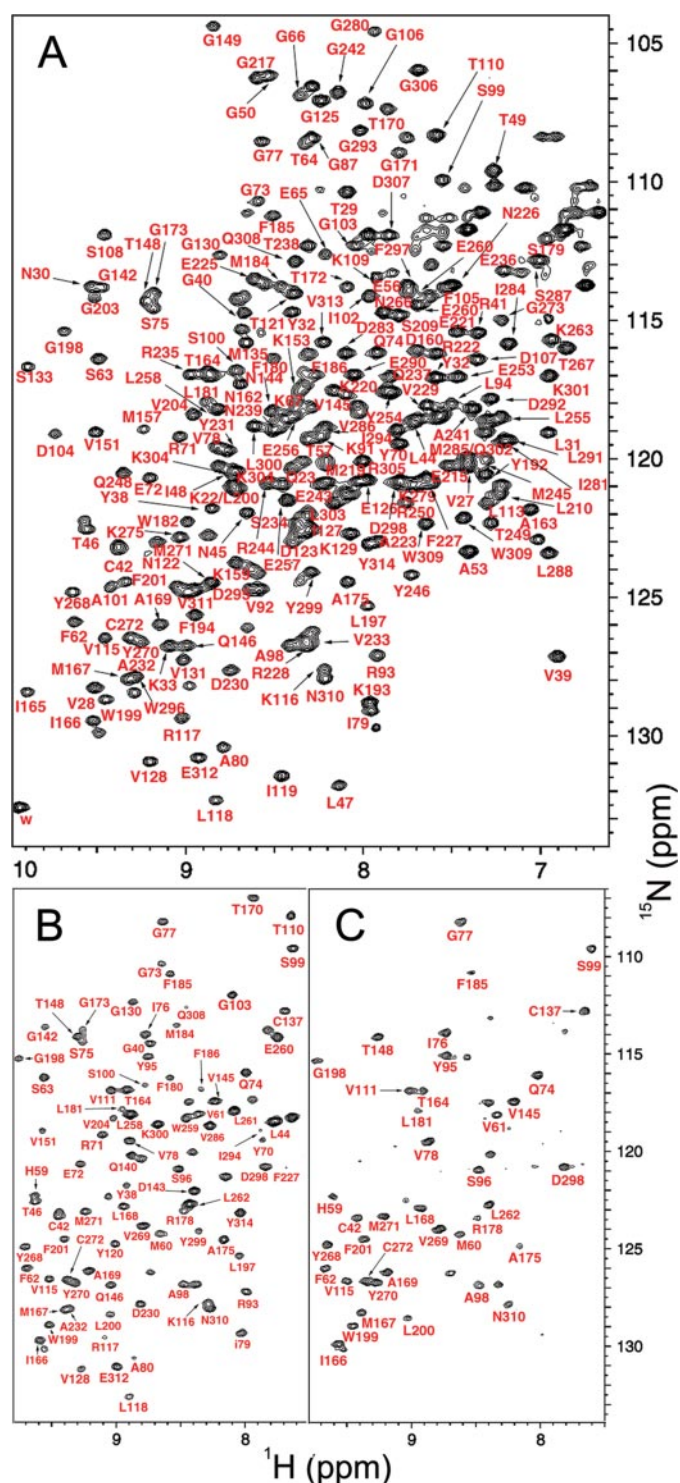
FIGURE 2. **H/D exchange experiments of FNR at 40 °C.** *A*, ^{1}H-^{15}N HSQC spectrum of uniformly ^{15}N-labeled FNR measured in a 25 mM sodium phosphate buffer at pH 8.0. Assignments of the backbone amide signals are indicated by the respective single-letter codes and residue numbers. The assignments of the Trp side chain indoles are labeled *w*. *B* and *C*, ^{1}H-^{15}N HSQC spectra measured during the H/D exchange experiments in a 25 mM *d*-sodium phosphate buffer at pD$_r$ 8.0. The spectra were acquired after 40 min (*B*) and 17 days (*C*) from the start of the exchange.

and making the first spectral measurement, many cross-peaks already disappeared (Fig. 2*B*). We confirmed that this rapid exchange was not caused by the dissolution of FNR (see below).
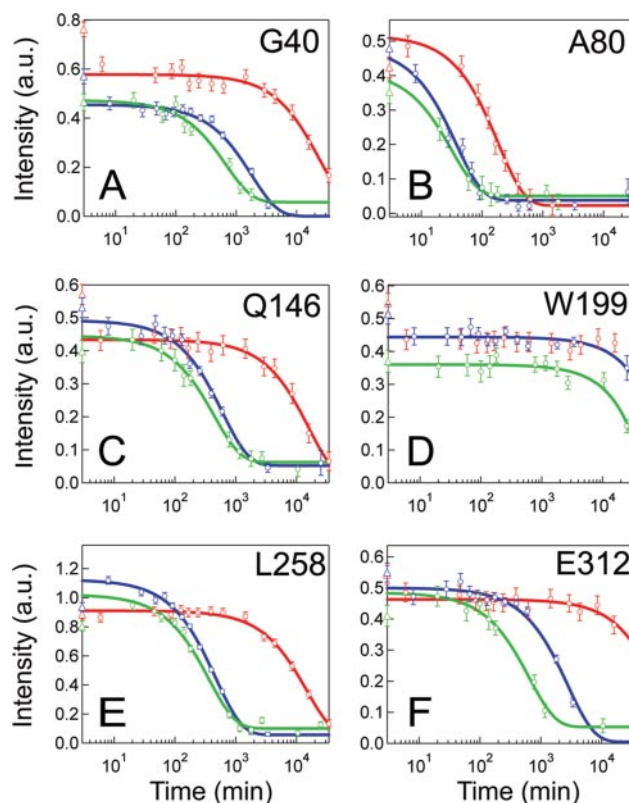
FIGURE 3. **Exchange kinetics for the representative residues of FNR.** Gly^{40} (*A*), Ala^{80} (*B*), Gln^{146} (*C*), Trp^{199} (*D*), Leu^{258} (*E*), and Glu^{312} (*F*) are shown. The peak intensities were plotted against the incubation time. The data were acquired at pD$_r$ 8.0 in the presence (*green*) or absence (*blue*) of 2.0 M *d*-urea and at pD$_r$ 6.0 (*red*). *Open triangles* at time 0 indicate the reference intensities measured in a H$_2$O solution. The fitting curves are also shown assuming a single exponential function where the exchange rate constant (k_{ex}) and initial and final intensities were adjustable parameters.

In contrast, even after 17 days of incubation, more than 40 peaks of strong intensity remained, indicating the presence of highly protected amide protons (Fig. 2*C*).

To accelerate the exchange, we added 2 M urea to the exchange buffer at pD$_r$ 8.0 and 40 °C, by which the protein was destabilized but still retained the native conformation even after 7 days (Fig. 1*B*). The overall exchange was accelerated in 2 M urea, although we still observed many intense peaks even after 17 days (supplemental Fig. S1*C*). These highly protected residues included Cys^{42} (β1), Met^{60} (β2), Tyr^{78} (β3), Tyr^{95} (β4), Val^{115} (β5), Cys^{137} (α1), and Val^{145} (β6) in the FAD-binding domain and Leu^{168} (β1), Met^{184} (α1), Phe^{201} (β2), Leu^{258} (α4), Cys^{272} (β4), Asp^{298} (α6), and Asn^{310} (β5) in the NADP$^+$-binding domain (see Figs. 4 and 5 and supplemental Table S2). These strongly protected residues were evidently located in the core secondary structure regions as shown by the x-ray structure, *i.e.* the six antiparallel β strands and the α1-helix in the FAD-binding domain as well as the central β strands (β1, β2, and β4) of the β-sheet and α1-helix in the NADP$^+$-binding domain. Judging from the peak intensities for methyl protons, most of the FNR remained in the native state after 17 days in the presence of 2 M urea.

The activity of FNR in chloroplasts (*i.e.* photoreduction of NADP$^+$) depends on the pH (15): whereas FNR is inactive at pH 6.0, it becomes more active with an increase of pH from 6.0 to
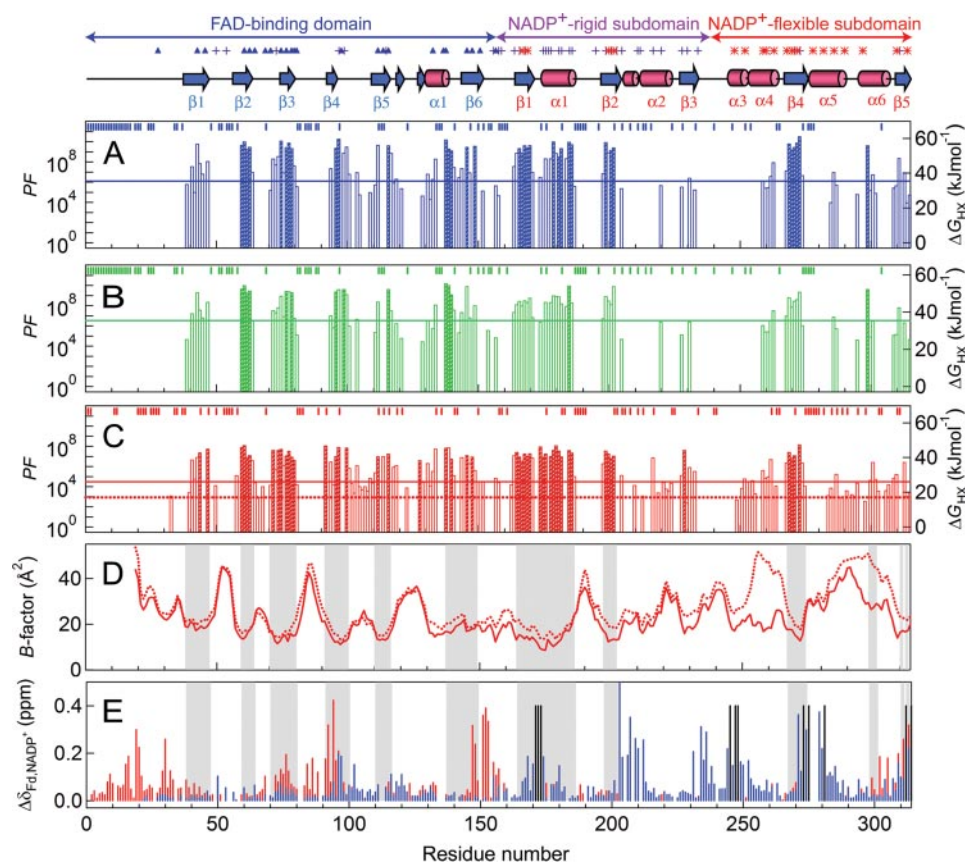
FIGURE 4. **Summary of PF values and comparison with other parameters.** *A–C,* PFs derived from the H/D exchange kinetics are plotted against the residue number. *A,* pD$_r$ 8.0. *B,* pD$_r$ 8.0 in the presence of 2.0 M *d*-urea. *C,* pD$_r$ 6.0. The unknown residues (see text) are marked with *short sticks* in the *upper part* of each panel. The upper limit residues are shown by *hatched bars.* The *right ordinate* indicates ΔG_{HX} estimated assuming the EX2 mechanism. The *horizontal solid lines* indicate the global ΔG_U values estimated from urea-induced denaturation under the corresponding conditions and the *red broken line* exhibits the ΔG_U value at pH 6.0 and 40 °C in the absence of 50 mM NaClO$_4$. The secondary structural elements determined on the basis of the x-ray structure (PDB entry 1GAW) are shown schematically in the *top.* Below the secondary structural scheme, secondary structures of FAD-binding and NADP$^+$-binding domains are labeled by *cyan* and *red letters,* respectively. Hydrophobic clusters (cluster I, ▲; cluster II, +; and cluster III, *) proposed by Bruns and Karplus (26) are marked *above* the secondary structural scheme. The locations of the FAD-binding domain and NADP$^+$-rigid and -flexible subdomains are indicated with *arrows* and *letters* in the uppermost part. *D,* B-factors obtained from the average values of the main-chain atoms (C$_\alpha$, N, C', O) are plotted with *solid* and *dotted lines* for each FNR conformer in a unit cell of a crystal obtained at pH 6.0 (see text). *E,* chemical shift perturbations (19) of FNR upon binding with ferredoxin at pH 6.0 (*red sticks*) and NADP$^+$ at pH 8.0 (*blue sticks*) are plotted against the residue number. *Black sticks* indicate the disappeared residues upon formation of the FNR-NADP$^+$ complex. The highly protected core regions are displayed with *shaded backgrounds* in *panels D* and *E.*

intensities against the incubation time (Fig. 3, supplemental Fig. S2). In all the H/D exchange experiments, the time ranges of exchanges widely varied depending on the residues. Generally, the reaction was faster in the order: pD$_r$ 8.0 in 2 M urea > pD$_r$ 8.0 in the absence of urea > pD$_r$ 6.0. In the absence of urea at pD$_r$ 8.0, among 269 assigned residues, 117 were exchanged completely within the first sampling period of 30 min, and are referred to as "the lower limit residues" (*i.e.* the protection is too low to quantify). In contrast, about 35 residues retained their initial peak intensities even after incubation for 17 days, and are referred to as "the upper limit residues" (*i.e.* the protection is too high to quantify). We excluded an additional 58 residues from the kinetic analysis, for which reliable data were not acquired because of a severe overlap of resonances or too large scattering of the peak intensity for unknown reasons, referring to them as "kinetics-undetermined residues." Consequently, the remaining 75 residues revealed a solid time-dependent decrease in peak intensity. For these residues, we assumed a first-order kinetics and fitted each time course to a single exponential curve, to estimate the apparent exchange rate constant (k_{ex}). Considering the presence of highly protected upper limit residues, the smallest k_{ex} one can determine here was about 2×10^{-6} min^{-1}, corresponding to 95% of intensity remaining after 17 days. On the other hand, the lower limit residues, with 5% of intensity left at 30 min, defined the largest k_{ex} to be about 0.1 min^{-1}.

Similar analyses were performed both at pD$_r$ 8.0 in the presence of 2 M urea and at pD$_r$ 6.0. The dead time measurements were 60 min at pD$_r$ 8.0 in the presence of 2 M urea and 50 min at pD$_r$ 6.0. The numbers of lower limit residues, residues that revealed the exchange rate constant, and upper limit residues were 128, 86, and 14, respectively, at pD$_r$ 8.0 in 2 M urea, and 81, 98, and 49, respectively, at pD$_r$ 6.0 (supplemental Figs. S1, S2, and Table S2). These numbers also indicate that the overall exchange was slower at pD$_r$ 6.0, suggesting that the intrinsic exchange rate, which increases along with pH, is an important factor for determining the observed kinetics.

To take into account the variation in the exchange rate depending on the type of amino acid residue and neighboring residues, we calculated the protection factor (PF) for each res-

8.0. This pH dependence is most likely to play a role in controlling the light-dependent circadian rhythm in stromas. To examine the effects of a pH shift on the conformational stability and dynamics of FNR, we further performed H/D exchange experiments at pD$_r$ 6.0 and 40 °C (supplemental Fig. S1, *B* and *C*). Here, we initiated the exchange reaction by diluting the concentrated FNR solution in H$_2$O with D$_2$O. The exchange pattern was generally similar to that at pD$_r$ 8.0, indicating that the method initiating the H/D exchange did not affect the observed kinetics. However, we found notable differences for several residues, particularly those located in the NADP$^+$-binding domain: whereas their peaks disappeared completely at the first measurement at pD$_r$ 8.0, the time course of exchanges could be followed at pD$_r$ 6.0.
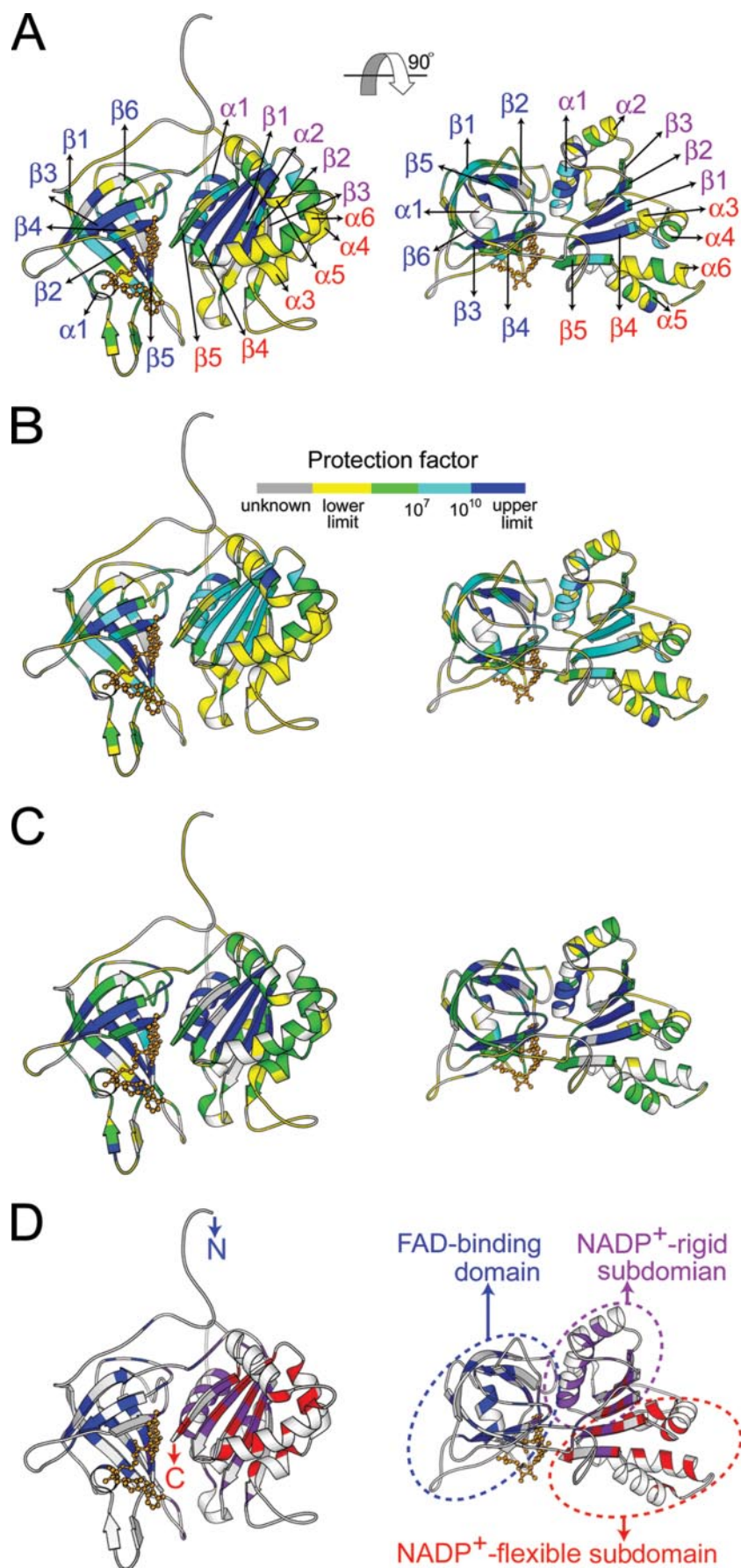
Estimation of Protection Factors—The exchange kinetics measured at pD$_r$ 8.0 in the presence and absence of 2 M urea as well as at pD$_r$ 6.0 was analyzed by plotting a series of peak

Protection factor

unknown | lower limit | 10^7 | 10^{10} | upper limit

FAD-binding domain

NADP⁺-rigid subdomian

NADP⁺-flexible subdomain

idue at pD_r 8.0 and 6.0. PF is defined as $k_{int}/k_{ex} = PF$, where k_{int} is the exchange rate constant in the random coil conformation (23, 25). The profile of PF against the residue number shows significant variation ranging from 10^3 and 10^{10} under the different conditions. Here, the lowest PF values to be determined assuming that 5% of peak intensity remains at the first time point are 10^4–10^5 at pD_r 8.0 and 10^2–10^3 at pD_r 6.0, where the range of PF is produced by the variation of k_{int}. For the same reason, the highest PF values to be determined with 95% of intensity remaining after an incubation period of 17 days at pD_r 8.0 are 10^8–10^{10} depending on the residues (supplemental Table S2). They are 10^6–10^8 at pD_r 6.0 according to 95% remaining intensity after 23 days. In other words, the true PF values of lower limit residues and upper limit residues can be smaller and larger, respectively, than these limiting values.

Protected Core Regions—The plots of PF against the residue number (Fig. 4) and on the three-dimensional schematic structure of FNR (Fig. 5) showed that the protected residues are clustered in various regions, which are well correlated with the location of the core secondary structures. FNR consists of FAD- and NADP$^+$-binding domains. The protected residues at pD_r 8.0 were obviously clustered on the six antiparallel β strands and one α-helix in the FAD-binding domain and on the five parallel β strands and two α-helices in the NADP$^+$-binding domain. In contrast, loop regions between α-helices and β strands and N- and C-terminal regions were least protected from exchange. FNR has a characteristic N-terminal region composed of 30 amino acid residues that form unstructured conformation as indicated by x-ray (16) and NMR analyses (20). The results of H/D exchange showing no protected residue in this region were consistent with the x-ray structure, confirming the flexibility in the N-terminal region.

In the FAD-binding domain, $\beta2$, $\beta3$, and $\beta4$ strands were the most strongly protected, forming the core of the β-barrel domain, whereas the $\alpha1$-helix was also considerably well protected. In the NADP$^+$-binding domain, parallel $\beta1$, $\beta2$, and $\beta4$ strands and $\alpha1$-helix were strongly protected, indicating less extensively protected core regions in comparison with the cores of the FAD-binding domain. In particular, $\alpha2$, $\alpha3$, and $\alpha5$ helices, forming the surface of the α/β-fold of the NADP$^+$-binding domain, were only marginally protected. On the other hand, $\alpha1$-helix of the NADP$^+$-binding domain, located at the interface between the two domains, was one of the most highly protected α-helices in FNR. This bipartic protection pattern suggests that the NADP$^+$-binding domain consists of two subdomains with distinct conformational dynamics (NADP$^+$-rigid and NADP$^+$-flexible subdomains, see "Discussion").

In the presence of 2 M urea at pD_r 8.0, PF decreased for many residues in comparison with values in the absence of urea (Figs. 4B and 5B). However, the extent of the acceleration of H/D exchange varied depending on the location of residues (Fig. 3): the residues in the NADP$^+$-binding domain tended to be exchanged faster than those in the FAD-binding domain, suggesting that the NADP$^+$-binding domain is preferentially destabilized in 2 M urea.

pD-dependent Conformational Change—Intrinsic exchange rates at pD_r 8.0 are 100-fold larger than those at pD_r 6.0. On the other hand, overall stability of FNR monitored based on CD or fluorescence measurements was slightly higher at pH 8.0 than at 6.0 (Fig. 1, supplemental Table S1). If the stability is independent of pD_r, the EX2 mechanism of H/D exchange (Ref. 10, see also "Discussion") predicts that, whereas the apparent exchange rate increases by a factor of 100 when the pD_r value is increased from 6.0 to 8.0, the PF values remain constant. The observed protection patterns throughout the entire backbone of FNR were similar at pD_r 6.0 and 8.0 with the PF values at pD_r 8.0 slightly larger than those at pD_r 6.0, as expected from the greater stability at pD_r 8.0 (Fig. 4).

In our case, the EX2 mechanism would be the first assumption to be discussed because k_{int} would be very large at both pD_r values, even though the mechanisms of H/D exchange for FNR have not been established: not all the exchanged residues exhibited an ideal pD_r-dependent increase in the exchange rate (supplemental Table S2 see "Discussion"). On the other hand, careful inspection of the PF values indicated that the $\alpha3$-helix, and the loops between $\alpha5$–$\alpha6$ and $\alpha6$–$\beta5$ in the NADP$^+$-binding domain were more protected at pD_r 6.0 than at pD_r 8.0: whereas many residues on the $\alpha3$–$\alpha6$ helices disappeared at the first point of the measurement (*i.e.* 40 min) at pD_r 8.0, their exchange kinetics could be followed at pD_r 6.0 revealing the PF values. This made the two subdomains of the NADP$^+$-binding domain distinguishable at pD_r 8.0, but unclear at pD_r 6.0.

DISCUSSION

Protected Core Regions and Two Subdomains of NADP$^+$-binding Domain—One of the most important results of the present study is that the H/D exchange at pD_r 8.0 revealed the presence of two subdomains in the NADP$^+$-binding domain: NADP$^+$-rigid and NADP$^+$-flexible subdomains. Bruns and Karplus (26) suggested the presence of three hydrophobic cores on the basis of the crystal structure of spinach leaf FNR, which are illustrated on the structure of maize leaf FNR (Fig. 5D). Cluster I located inside of the six-stranded β-barrel corresponds to the core of the FAD-binding domain. The NADP$^+$-binding domain contains two hydrophobic clusters, clusters II and III. Cluster II includes the interface between the two major domains and the N-terminal part of the NADP$^+$-binding domain. Cluster III, located on the far side of the parallel β-sheet, includes the C-terminal part of the NADP$^+$-binding domain. The profiles of PF were consistent with the hydrophobic clusters suggested by Bruns and Karplus (26) (Figs. 4 and 5) and, moreover, suggest the presence of two subdomains, each including one of these hydrophobic clusters. The NADP$^+$-flexible subdomain, rich in

FIGURE 5. **Mapping of the PFs and cores on the crystal structures.** *A–C*, PFs acquired at pD_r 8.0 in the absence (*A*) or presence (*B*) of 2.0 M *d*-urea and at pD_r 6.0 (*C*). The colors represent the different PFs: unknown PF (*gray*), PF in the lower limit (*yellow*), PF $< 10^7$ (*green*), $10^7 <$ PF $< 10^{10}$ (*cyan*), and PF in the upper limit (*navy blue*). The unknown residues include the unassigned residues and the kinetics-undetermined residues. *D*, hydrophobic clusters suggested by Bruns and Karplus (26) are colored in *blue* (cluster I), *magenta* (cluster II), and *red* (cluster III). The FAD molecule is displayed as an *orange* ball-and-stick model. The *right figures* were drawn by rotating the left one along the indicated axis by 90°. The three-dimensional structures were drawn by MOLSCRIPT (46) with the crystal structure (PDB entry 1GAW).

α-helices, had more dynamic regions, as shown by Figs. 4 and 5, than the NADP$^+$-rigid subdomain, except for β_4 strand.

Although the typical Rossmann fold (18) is made of two structural mononucleotide binding motifs, *i.e.* a repeat of a β-α-β-α-β motif constituting a parallel six-stranded β-sheet with symmetrical α-helices on both sides of the sheet with relative strand order $\beta_3\beta_2\beta_1\beta_4\beta_5\beta_6$ (27), the NADP$^+$-binding domain of maize leaf FNR has a variant topology. To be more precise, the NADP$^+$-rigid subdomain retains pairs of the typical β-α-β-α-β motif (*i.e.* $\beta_1\alpha_1\beta_2\alpha_2\beta_3$) with relative strand order $\beta_3\beta_2\beta_1$. On the other hand, the NADP$^+$-flexible subdomain has a $\alpha_3\alpha_4\beta_4\alpha_5\alpha_6\beta_5$ topology with relative strand order $\beta_4\beta_5$, lacking one strand corresponding to β_6, including two additional α-helices (Fig. 4). There are several reports describing that the regions of the NADP$^+$-flexible subdomain is not the typical Rossmann fold (26, 28), which are in accordance with our observation.

Our classification of the NADP$^+$-binding domain into two subdomains is strongly supported by limited proteolysis studies of spinach FNR, reporting that the NADP$^+$-flexible subdomain could be cleaved from the NADP$^+$-binding domain (29, 30). Two subdomains are connected by both hydrophobic interactions through the β_4 strand and surface-exposed flexible loop region that contains a protease active site. In addition, the proposals that a domain should contain a hydrophobic core as an independent folding unit (31, 32) and that compactness without a hydrophobic core alone does not determine the presence of a domain (33) also provide us with reliable grounds for the division of the NADP$^+$-binding domain into the two subdomains.

pH-dependent Change in Dynamics of the NADP$^+$-flexible Subdomain—Because illumination of intact chloroplasts increases the stromal pH from about 6 to 8 (15), it has been suggested that the light-driven increase in pH induces a conformational change in FNR, which leads to the increase in its reductase activity and also in the affinity for its substrate, NADP$^+$. Although a study using chemical modifications suggested the presence of the essential carboxyl group at the nucleotide-binding site (34), no detailed structure-based information in solution is available to date. The present study showed that the dynamics of the NADP$^+$-flexible subdomain, particularly of the four α-helices, increased in response to a pD$_r$ change from 6.0 to 8.0 (*i.e.* from night to daytime), suggesting that this elevated dynamics is responsible for the enhanced affinity of FNR for NADP$^+$.

A large number of reports describing the consequences of increased dynamic motions in enzymes to their elevated activities are in accordance with our results. In the case of FNR, the most mobile part in a crystal structure revealed by the *B* factor falls into the NADP$^+$-flexible subdomain (26, 28). This part also corresponds to the structurally most varied regions among six distinct crystal structures of FNRs (28). Furthermore, two conformers of maize leaf FNR were found in a unit cell of the crystal prepared at pH 6.0. The *B* factors in the NADP$^+$-flexible subdomain in the two conformers differ considerably (Fig. 4D) (16), and this motional difference in crystals is consistent with the difference in our PF profiles in solution at pD$_r$ 8.0 and 6.0. In addition, most of the residues of FNR that were largely per-

turbed in their chemical shifts upon binding of NADP$^+$ at pH 8.0 existed in the NADP$^+$-flexible subdomain, suggesting that the motional mode is important for the substrate binding (Fig. 4E), whereas the largely perturbed residues upon formation of the Fd-FNR complex are mostly in the FAD-binding domain (Fig. 4E) (20).

The higher dynamic motion in the NADP$^+$-flexible subdomain at pD$_r$ 8.0 than at pD$_r$ 6.0 is most likely to facilitate rapid sampling in the conformational space for selecting the most suitable conformation for enhancing the binding affinity for NADP$^+$, especially in the first binding step of the adenosine portion of NADP$^+$ in the bipartite NADP$^+$ binding mode (20, 35). The fact that the presence of NADP$^+$ at the active site is a prerequisite for the catalysis of FNR (35) can explain why the NADP$^+$-flexible subdomain exhibits the higher motional behavior than other regions of FNR at pD$_r$ 8.0. Taken together, we postulate that binding of NADP$^+$ to the NADP$^+$-flexible subdomain may trigger a change of motional mode in the Fd-binding site through a dynamic network, facilitating a higher affinity to Fd and increasing ultimately the overall catalytic cycle. Although it is not clear whether H/D exchange occurs through small scale motion (*i.e.* local fluctuation) or large scale motion (*i.e.* subglobal or global unfoldings), the different motional modes in the NADP$^+$-flexible subdomain at the two pD$_r$ values probably control the binding affinity for NADP$^+$. On the other hand, FNR needs to be stable during catalysis for sustaining its native structure. Therefore, rigid β_4 strand seems important for maintaining stability of both the NADP$^+$-flexible subdomain as the small core and the NADP$^+$-rigid subdomain through hydrophobic interaction with β_1 strand that is directly adjacent to the NADP$^+$-flexible subdomain in space (Fig. 5). Consequently, the structure of the NADP$^+$-flexible subdomain is dynamic in retaining the rigid small β_4 strand. Our results are consistent with the fact that an enzyme needs to be both stable to maintain their native structures and flexible to allow conformational changes during catalysis (36). Considering evolution of enzymes for pH sensitivity, achieved by tuning the local motion (37), the pH-modulated change in motion of the NADP$^+$-flexible subdomain may be achieved through evolution for photosynthesis.

Free Energy Change of Unfolding—PFs obtained from the H/D exchange experiment can be related to the parameters of protein unfolding at each amide site, assuming a two-state transition model between the folded (N) and unfolded (U) states and the exchanged state (X),

$$N \underset{k_R}{\overset{k_U}{\rightleftarrows}} U \overset{k_{int}}{\longrightarrow} X$$
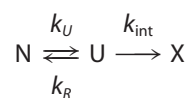
SCHEME 1

where k_U and k_R represent the unfolding and refolding rate constants, respectively (38, 39). The equilibrium constant (K_U) between N and U is related to the microscopic rate constants by $K_U = k_U/k_R$. Under conditions where the conformational equilibrium is much faster than the intrinsic rate of exchange ($k_R \gg k_{int}$, EX2 limit), the apparent exchange rate constant (k_{ex}) is represented by $K_U k_{int}$. Here, PF corresponds to $1/K_U$ and ΔG_{HX}

equals $RT \ln PF$. Under the other extreme condition where k_{int} is much higher than the refolding rate constant k_R, k_{ex} represents k_U (EX1 limit).

Generally for smaller proteins, assuming the EX2 mechanism (see "Results"), the highest ΔG_{HX} value estimated by H/D exchange corresponds to the overall ΔG_U value calculated from the unfolding transition curve obtained with denaturants or with heat (39–42). On the other hand, there are some possible contributions to the increase in the ΔG_{HX} value, such as the existence of superprotected residues (43), the effects of solvent isotopes (by $\pm 0 - 2$ kcal/mol), and proline isomerization (44, 45).

Although we do not know the true ΔG_U for FNR, because the global unfolding is apparently irreversible, it is evident that conventional methods including an analysis of the apparent unfolding transition curve significantly underestimate ΔG_U. Indeed, the ΔG_{HX} values of many residues were greater than the apparent ΔG_U values obtained from CD or fluorescence measurements. Nevertheless, we could not determine the exact PF values for highly protected residues in the tight core regions and consequently the ΔG_{HX} value for global unfolding, suggesting only the lower limit of the real ΔG_{HX} value. Considering various unknown factors including the presence of superprotected residues and the solvent isotope effects enhancing the apparent stability of FNR, further studies are required to determine the exact correlation of global unfolding with the observed PF.

Conclusions—As far as we know, this is the largest protein for which a detailed analysis of H/D exchange has been performed, and the first site-specific study on the pH-modulated relationship between dynamics and function on FNR-type flavoenzyme in solution. We determined the motion of the molecule for each residue and its dependence on pH, revealing that the NADP$^+$-binding domain is made of two subdomains different in their dynamic behaviors. We suggest that the pH-dependent change in motion of the NADP$^+$-flexible subdomain is important for controlling the binding affinity of FNR for NADP$^+$, leading to the effective catalytic cycle of photosynthesis. The H/D exchange experiments provided the ΔG_{HX} values assuming the EX2 mechanism. Although the ΔG_{HX} values for highly protected residues are minimal and the real values might be larger, even defining the minimal values is of paramount importance for addressing the structural dynamics of large proteins for which no other approach is available at the moment.

REFERENCES

1. Kay, L. E. (1998) *Nat. Struct. Biol.* **5,** 513–517
2. Ishima, R., and Torchia, D. A. (2000) *Nat. Struct. Biol.* **7,** 740–743
3. Steensma, E., and van Mierlo, C. P. M. (1998) *J. Mol. Biol.* **282,** 653–666
4. Polshakov, V. I., Birdsall, B., and Feeney, J. (2006) *J. Mol. Biol.* **356,** 886–903
5. Gozu, M., Hoshino, M., Higurashi, T., Kato, H., and Goto, Y. (2002) *Protein Sci.* **11,** 2792–2803
6. Clake, J., and Itzhaki, L. S. (1998) *Curr. Opin. Struct. Biol.* **8,** 112–118
7. Katou, H., Hoshino, M., Kamikubo, H., Batt, C. A., and Goto, Y. (2001) *J. Mol. Biol.* **310,** 471–484
8. Williams, D. H., Stephens, E., O'Brien, D. P., and Zhou, M. (2004) *Angew. Chem. Int. Ed.* **43,** 6569–6616
9. Popovych, N., Sun, S., Ebright, R. H., and Kalodimos, C. G. (2006) *Nat. Struct. Mol. Biol.* **9,** 831–838
10. Milne, J. S., Xu, Y., Mayne, L. C., and Englander, S. W. (1999) *J. Mol. Biol.* **290,** 811–822
11. Li, R., and Woodward, C. (1999) *Protein Sci.* **8,** 1571–1591
12. Lu, J., and Dahlquist, F. W. (1992) *Biochemistry* **31,** 4749–4756
13. Freund, C., Honegger, A., Hunziker, P., Holak, T. A., and Plückthun, A. (1996) *Biochemistry* **35,** 8457–8464
14. Arakaki, A. K., Ceccarelli, E. A., and Carrillo, N. (1997) *FASEB J.* **11,** 133–140
15. Carrillo, N., Lucero, H. A., and Vallejos, R. H. (1981) *J. Biol. Chem.* **256,** 1058–1059
16. Kurisu, G., Kusunoki, M., Katoh, E., Yamazaki, T., Teshima, K., Onda, Y., Kimita-Ariga, Y., and Hase, T. (2001) *Nat. Struct. Biol.* **8,** 117–121
17. Karplus, P. A., Walsh, K. A., and Herriott, J. R. (1991) *Science* **251,** 60–66
18. Rossman, M., Moras, D., and Olsen, K. (1974) *Nature* **250,** 194–199
19. Maeda, M., Hamada, D., Hoshino, M., Onda, Y., Hase, T., and Goto, Y. (2002) *J. Biol. Chem.* **277,** 17101–17107
20. Maeda, M., Lee, Y. H., Ikegami, T., Tamura, K., Hoshino, M., Yamazaki, T., Nakayama, M., Hase, T., and Goto, Y. (2005) *Biochemistry* **44,** 10644–10653
21. Pace, C. N. (1986) *Methods Enzymol.* **131,** 266–280
22. Delaglio, F., Grzesiek, S., Vuister, G., Zhu, G., Pfeifer, J., and Baz, A. (1995) *J. Biomol. NMR* **6,** 277–293
23. Bai, Y., Milne, J. S., and Englander, S. W. (1993) *Proteins* **17,** 75–86
24. Shortle, D., Meeker, A. K., and Gerring, S. L. (1989) *Arch. Biochem. Biophys.* **272,** 103–113
25. Connelly, G. P., Bai, Y., Jeng, M.-F., and Englander, S. W. (1993) *Proteins* **17,** 87–92
26. Bruns, C. M., and Karplus, P. A. (1995) *J. Mol. Biol.* **247,** 125–145
27. Bottoms, C. A., Smith, P. E., and Tanner, J. J. (2002) *Protein Sci.* **11,** 2125–2137
28. Karplus, P. A., and Faber, H. R. (2004) *Photosynth. Res.* **81,** 303–315
29. Gadda, G., Aliverti, A., Ronchi, S., and Zanetti, G. (1990) *J. Biol. Chem.* **265,** 11955–11959
30. Aliverti, A., Pandini, V., and Zanetii, G. (2004) *Biochim. Biophys. Acta* **1696,** 93–101
31. Swindells, M. B. (1995) *Protein Sci.* **4,** 103–112
32. Zehfus, M. H. (1995) *Protein Sci.* **4,** 1188–1202
33. Zehfus, M. H. (1997) *Protein Sci.* **6,** 1210–1219
34. Carrillo, N., Arana, J. L., and Vallejos, R. H. (1981) *J. Biol. Chem.* **256,** 6823–6828
35. Carrillo, N., and Ceccarelli, E. A. (2003) *Eur. J. Biochem.* **270,** 1900–1915
36. Höcker, B., Jürgens, C., Wilmanns, M., and Sterner, R. (2001) *Curr. Opin. Biotechnol.* **12,** 376–381
37. Whitten, S. T., Garcia-Moreno, E. B., and Hilser, V. J. (2005) *Proc. Natl. Acad. Sci. U. S. A.* **102,** 4282–4287
38. Englander, S. W., Sosnick, T. R., Englander, J. J., and Mayne, L. (1996) *Curr. Opin. Struct. Biol.* **6,** 18–23
39. Loh, S. N., Prehoda, K. E., Wang, J., and Markley, J. L. (1993) *Biochemistry* **32,** 11022–11028
40. Mayo, S. L., and Baldwin, R. L. (1993) *Science* **262,** 873–876
41. Clarke, J., Hounslow, A. M., Bycroft, M., and Fersht, A. R. (1993) *Proc. Natl. Acad. Sci. U. S. A.* **90,** 9837–9841
42. Jandu, S. K., Ray, S., Brooks, L., and Leatherbarrow, R. J. (1990) *Biochemistry* **29,** 6264–6269
43. Swint, L., and Robertson, A. D. (1996) *Biochemistry* **35,** 171–180
44. Cioni, P., and Strambini, G. B. (2002) *Biophys. J.* **82,** 3246–3253
45. Huyghues-Despointes, B. M., Pace, C. N., Englander, S. W., and Scholtz, J. M. (2001) *Methods Mol. Biol.* **168,** 69–92
46. Kraulis, P. J. (1991) *J. Appl. Crystallogr.* **24,** 946–950

Cores and pH-dependent Dynamics of Ferredoxin-NADP$^+$ Reductase Revealed by Hydrogen/Deuterium Exchange

Young-Ho Lee, Kosuke Tamura, Masahiro Maeda, Masaru Hoshino, Kazumasa Sakurai, Satoshi Takahashi, Takahisa Ikegami, Toshiharu Hase and Yuji Goto

Access the most updated version of this article at doi: 10.1074/jbc.M608417200

Alerts:
- When this article is cited
- When a correction for this article is posted

Click here to choose from all of JBC's e-mail alerts

Supplemental material:
http://www.jbc.org/content/suppl/2006/12/28/M608417200.DC1

This article cites 44 references, 8 of which can be accessed free at
http://www.jbc.org/content/282/8/5959.full.html#ref-list-1

CORES AND pH-DEPENDENT DYNAMICS OF FERREDOXIN−NADP+ REDUCTASE REVEALED BY H/D EXCHANGE

Young-Ho Lee, Kosuke Tamura, Masahiro Maeda, Masaru Hoshino, Kazumasa Sakurai, Satoshi

Takahashi, Takahisa Ikegami, Toshiharu Hase and Yuji Goto

Supplemental Figure S1. **H/D exchange experiments of FNR measured in 25 mM *d*-sodium phosphate at pD$_r$ 8.0 in the presence of 2.0 M *d*-urea (A, C) and at pD$_r$ 6.0 (B, D).** The spectra were acquired after 50 min (A), 17 days (C), 40 min (B), and 20 days (D) from the start of the exchange.
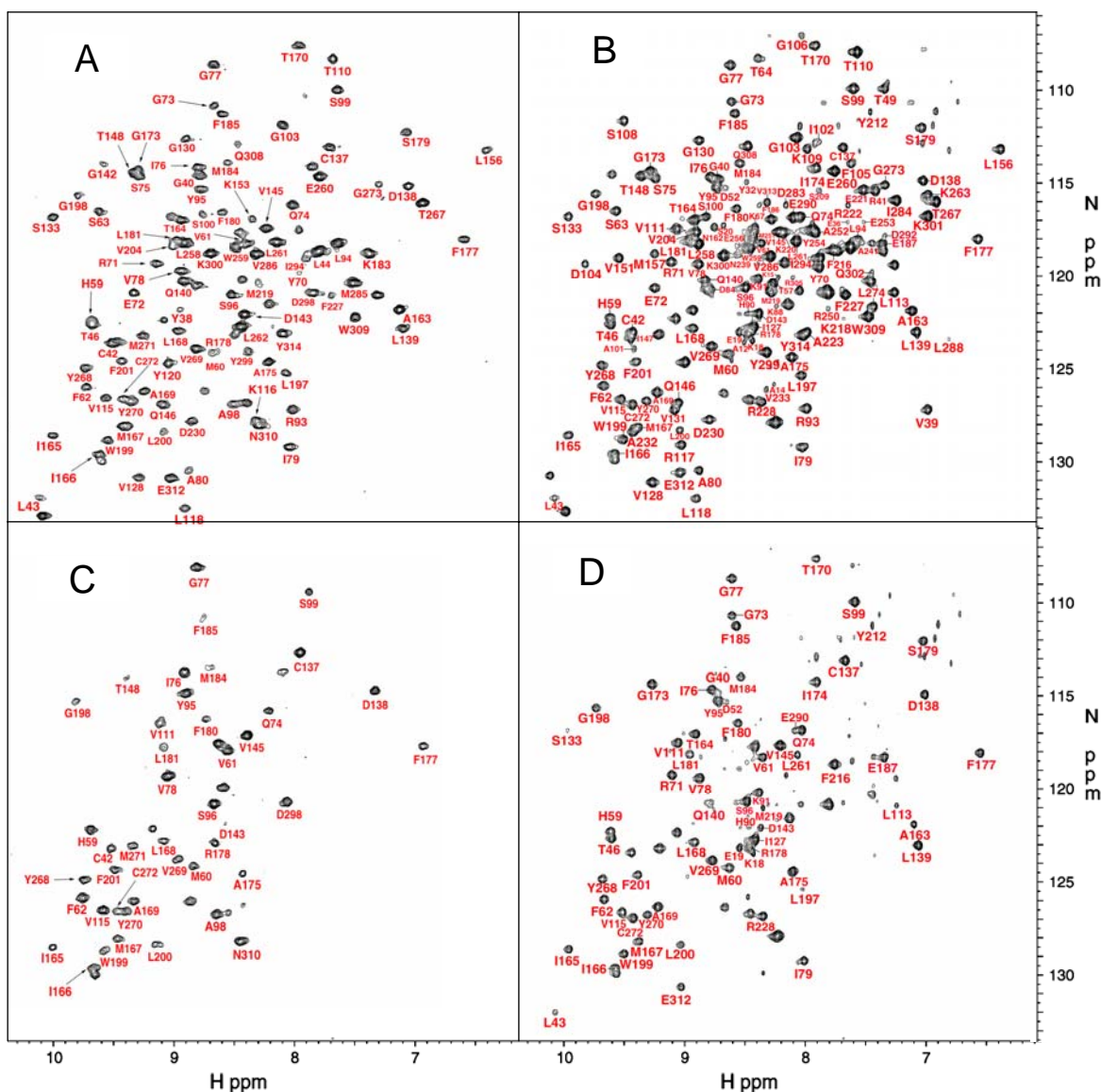
Supplemental Figure S2.   H/D exchange kinetics for the respective residues of FNR.   The data were acquired at pD_r 8.0 in the presence (green) and absence (blue) of 2.0 M d-urea as well as at p$\underline{D}_r$ 6.0 (red). The peak intensities were plotted as a function of the incubation times, and lines are fitting curves derived assuming a single exponential function with an exchange rate constant (k_{ex}).   The residues including ambiguity are indicated by asterisks at the left side of a single-letter code.   The upper limit (triangles) and lower limit (inverted triangles) residues are marked by closed symbols at the left side of a single-letter code instead of a solid fitting line, and among these residues the ambiguously-selected cases are shown by the open symbols.   Small closed triangles on the left ordinate are the reference intensities in H_2O solution. The inset for M219 is a close-up view of the range of intensities.
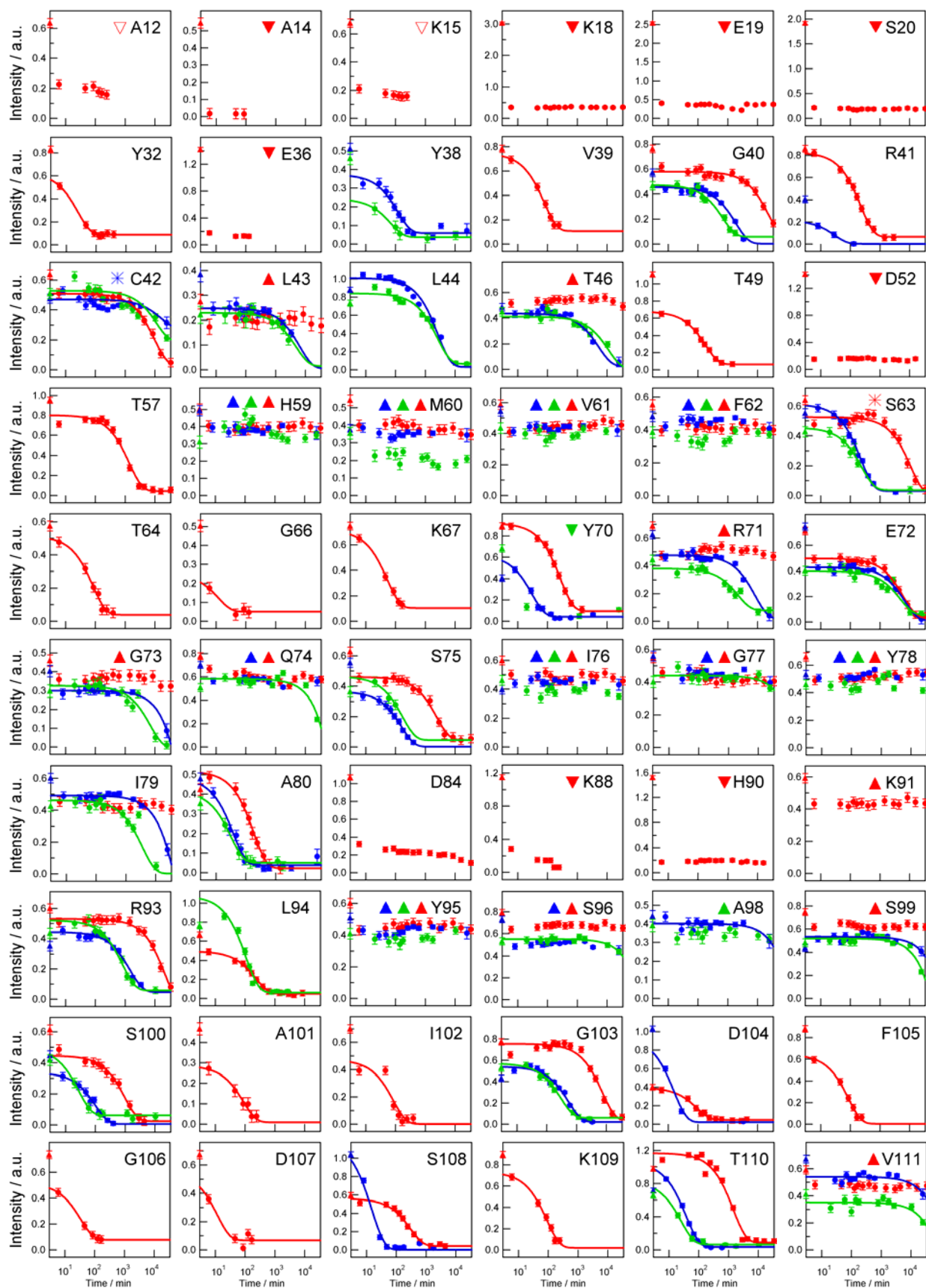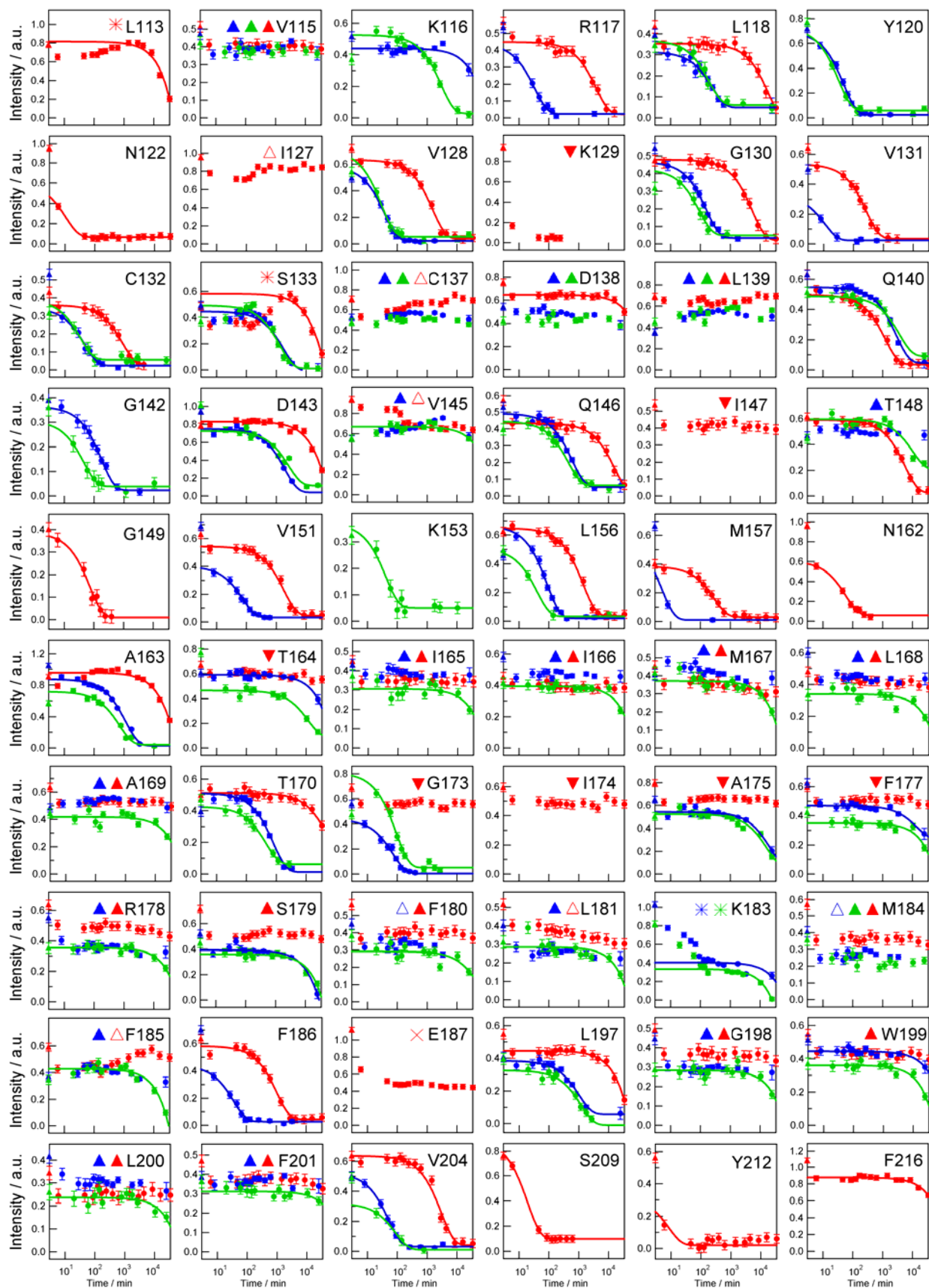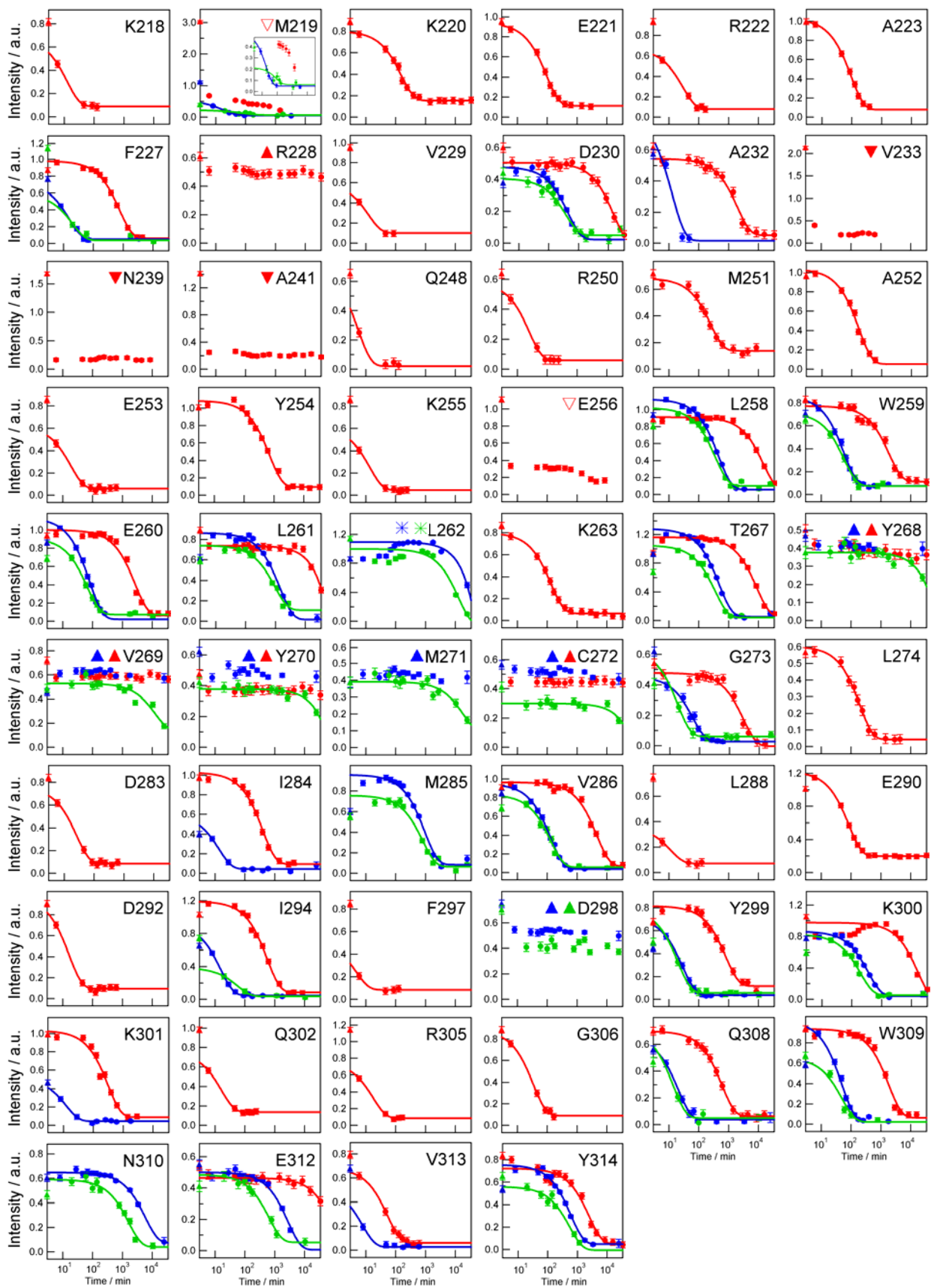
Supplemental Table S1.   Apparent thermodynamic parameters for the unfolding of FNR.

Conditions	Incubation time (day)	Temp (ºC)	ΔG_U^{a} (kJ·mol^{-1})	M^{b} (kJ·mol^{-1}·M^{-1})	C_m^{c} (M)
Urea-induced unfolding at pH 8.0	1[d]	25	39.6 ± 2.1	6.7 ± 0.4	5.9
	1[e]	25	33.6 ± 2.3	5.7 ± 0.4	5.9
	1[d]	40	35.4 ± 2.6	9.1 ± 0.7	3.9
	1[e]	40	33.0 ± 2.8	8.2 ± 0.7	4.0
	3[e]	40	24.4 ± 2.8	6.5 ± 0.7	3.8
	7[e]	40	10.8 ± 2.3	4.0 ± 0.8	2.7
Urea-induced unfolding at pH 6.0 and 50 mM NaClO$_4$.	1[e]	40	26.4 ± 3.1	6.9 ± 0.8	3.8
	3[e]	40	23.1 ± 4.3	6.9 ± 0.1	3.3
	7[e]	40	16.9 ± 3.7	6.9 ± 0.1	2.5
Urea-induced unfolding at pH 6.0	1[e]	40	17.3 ± 2.6	4.7 ± 0.7	3.7
	3[e]	40	15.3 ± 2.7	4.4 ± 0.7	3.5
	7[e]	40	8.4 ± 2.5	2.7 ± 0.5	2.6
Gdn-HCl-induced unfolding at pH 6.0[1]	0.17[d]	10	9.2 ± 1.9	4.5 ± 0.9	2.0
	0.17[e]	10	9.2 ± 1.1	4.3 ± 0.5	2.1

[a]Free energy change of unfolding obtained by an extrapolation to zero denaturant concentration.

[b]Cooperativity index of the transition.

[c]Midpoint urea concentration of unfolding.

[d]Data obtained by CD at 222 nm.

[e]Data obtained with fluorescence at 530 nm.

1. Maeda, M., Hamada, D., Hoshino, M., Onda, Y., Hase, T., and Goto, Y. (2002) *J. Biol. Chem.* **277**, 17101-17107

Supplemental Table S2. Summary of the H/D exchange of FNR.

[a]Superscripts I, II, and III indicate hydrophobic cores I; II, and III, respectively.

[b]FD, FAD-binding domain; NRD, NADP$^+$-rigid subdomain; and NFD, NADP$^+$-flexible subdomain.

[c]A, α-helix; B, β-strand; and L, loop

[d]Bold and italic letters indicate the upper limit residues and the residues with fitting ambiguity, respectively. LO indicates lower limit residue. For the residues with a slash, the exchange rate was not determined because of no assignment as marked with [e] or because of a failure to acquire reliable data (i.e., kinetics-undetermined residue) for those without a mark.

Residue number[a]	(Sub) Domain[b]	Secondary structure[c]	pD$_r$ 8.0[d]			pD$_r$ 8.0 in 2M urea[d]			pD$_r$ 6.0[d]		
			logk_{int}	logk_{ex}	logPF	logk_{int}	logk_{ex}	logPF	logk_{int}	logk_{ex}	logPF
I1	FD	L		—[e]			—[e]			—[e]	
R2	FD	L	4.5	—[e]		4.5	—[e]		3.6	—	
A3	FD	L	4.4	—[e]		4.4	—[e]		2.4	LO	
Q4	FD	L	4.3	—[e]		4.3	—[e]		2.3	LO	
A5	FD	L	4.4	—[e]		4.4	—[e]		2.4	LO	
S6	FD	L	4.6	—[e]		4.6	—[e]		2.6	LO	
A7	FD	L	4.5	—[e]		4.5	—[e]		2.5	LO	
V8	FD	L	3.5	—[e]		3.5	—[e]		1.5	LO	
E9	FD	L	3.5	—[e]		3.5	—[e]		1.6	LO	
A10	FD	L	4.0	—[e]		4.0	—[e]		2.0	LO	
P11	FD	L		—[e]			—[e]			—[e]	
A12	FD	L	4.0	—[e]		4.0	—[e]		2.0	*LO*	
T13	FD	L	4.1	—[e]		4.1	—[e]		2.1	LO	
A14	FD	L	4.4	—[e]		4.4	—[e]		2.4	LO	
K15	FD	L	4.2	—[e]		4.2	—[e]		2.2	*LO*	
A16	FD	L	4.3	—[e]		4.3	—[e]		2.3	LO	
K17	FD	L	4.2	—[e]		4.2	—[e]		2.2	LO	
K18	FD	L	4.3	LO		4.3	LO		2.3	LO	
E19	FD	L	3.8	—		3.8	—		1.8	LO	
S20	FD	L	4.4	—		4.4	—		2.4	—	
K21	FD	L	4.5	—		4.5	—		2.5	—	

Residue											
K22	FD	L	4.3	LO		4.3	LO		2.3	—	
Q23	FD	L	4.4	LO		4.4	LO		2.4	—	
E24	FD	L	3.9	—		3.9	—		1.9	LO	
E25	FD	L	3.5	—		3.5	—		1.6	—	
G26	FD	L	4.3	—[e]		4.3	—[e]		2.3	—[e]	
[I]V27	FD	L	3.7	LO		3.7	LO		1.7	—	
V28	FD	L	3.4	LO		3.4	LO		1.4	—	
T29	FD	L	4.0	LO		4.0	LO		2.0	LO	
N30	FD	L	4.9	LO		4.9	LO		2.9	LO	
L31	FD	L	3.9	LO		3.9	LO		1.9	LO	
Y32	FD	L	3.7	LO		3.7	LO		1.7	-1.4	3.1
L33	FD	L	4.2	LO		4.2	LO		2.2	LO	
P34	FD	L		—[e]			—[e]			—[e]	
K35	FD	L	3.9	—		3.9	—		1.9	—	
E36	FD	L	3.8	LO		3.8	LO		1.8	LO	
P37	FD	L		—[e]			—[e]			—[e]	
Y38	FD	B1	3.7	-2.1	5.8	3.7	-1.0	4.7	1.7	—	
V39	FD	B1	3.5	LO		3.5	LO		1.5	-1.9	3.4
G40	FD	B1	4.3	-3.2	7.6	4.3	-2.9	7.2	2.3	-4.4	6.7
R41	FD	B1	4.4	-0.6	5.0	4.4	LO		2.4	-2.4	4.8
[I]C42	FD	B1	5.0	*-4.8*	*9.8*	5.0	-4.4	9.3	3.0	-4.0	6.9
L43	FD	B1	4.1	-3.8	7.9	4.1	-3.5	7.6	2.1	**-5.3**	**7.4**
L44	FD	B1	3.4	-3.4	6.8	3.4	-3.4	6.8	1.4	—	
[I]N45	FD	B1	4.5	LO		4.5	LO		2.5	LO	
T46	FD	B1	4.4	-3.6	8.1	4.4	-3.9	8.4	2.4	**-5.3**	**7.8**
K47	FD	B1	4.4	LO		4.4	LO		2.4	—	
I48	FD	L	3.6	—		3.6	—		1.6	LO	
[II]T49	FD	L	3.9	LO		3.9	LO		1.9	-2.3	4.1
G50	FD	L	4.7	LO		4.7	LO		2.7	—	
D51	FD	L	4.1	—		4.1	—		2.1	LO	
D52	FD	L	3.7	—		3.7	—		1.7	LO	
[II]A53	FD	L	4.0	LO		4.0	LO		2.0	—	

Residue											
P54	FD	L		—e			—e			—e	
G55	FD	L	4.2	—		4.2	—		2.2	—	
E56	FD	L	3.9	—		3.9	—		1.9	—	
T57	FD	B2	4.0	LO		4.0	LO		2.0	-3.1	5.1
W58	FD	B2	4.0	—e		4.0	—e		2.0	—e	
H59	FD	B2	4.0	**-5.7**	**9.7**	4.0	**-5.7**	**9.7**	2.6	**-5.3**	**7.9**
[I]M60	FD	B2	4.3	**-5.7**	**10**	4.3	**-5.7**	**10**	2.8	**-5.3**	**8.1**
V61	FD	B2	3.6	**-5.7**	**9.3**	3.6	**-5.7**	**9.3**	1.6	**-5.3**	**6.9**
[I]F62	FD	B2	3.8	**-5.7**	**9.5**	3.8	**-5.7**	**9.5**	1.8	**-5.3**	**7.1**
S63	FD	B2	4.6	-2.4	7.0	4.6	-1.9	6.5	2.6	*-4.0*	6.6
[I]T64	FD	L	4.4	LO		4.4	LO		2.4	-2.0	4.4
E65	FD	L	3.9	LO		3.9	LO		1.9	LO	
G66	FD	L	4.3	LO		4.3	LO		2.3	-0.6	3.0
K67	FD	L	4.3	LO		4.3	LO		2.3	-1.7	4.0
[I]I68	FD	L	3.6	LO		3.6	LO		1.6	LO	
P69	FD	L		—e			—e			—e	
[I]Y70	FD	L	3.7	-1.5	5.2	3.7	LO		1.7	-2.5	4.2
R71	FD	L	4.3	-4.0	8.3	4.3	-3.2	7.6	2.3	**-5.3**	**7.6**
[II]E72	FD	L	3.9	-3.8	7.7	3.9	-3.4	7.3	1.9	-3.8	5.7
G73	FD	L	4.3	-4.3	8.6	4.3	-3.5	7.8	2.3	**-5.3**	**7.6**
[I]Q74	FD	L	4.4	**-5.7**	**10**	4.4	-4.6	9.0	2.4	**-5.3**	**7.7**
S75	FD	B3	4.8	-2.2	7.0	4.8	-2.2	7.0	2.8	-3.4	6.1
[I]I76	FD	B3	3.8	**-5.7**	**9.5**	3.8	**-5.7**	**9.5**	1.8	**-5.3**	**7.1**
G77	FD	B3	4.2	**-5.7**	**9.9**	4.2	-5.2	9.4	2.2	**-5.3**	**7.6**
[I]Y78	FD	B3	3.7	**-5.7**	**9.4**	3.7	**-5.7**	**9.4**	1.7	**-5.3**	**7.0**
[I]I79	FD	B3	3.3	-4.3	7.6	3.3	-3.5	6.8	1.3	**-5.3**	**6.6**
[I]A80	FD	L	4.0	-1.6	5.6	4.0	-1.2	5.2	2.0	-2.3	4.2
D81	FD	L	3.9	—e		3.9	—e		1.9	—e	
G82	FD	L	4.3	—		4.3	—		2.3	—	
V83	FD	L	3.7	LO		3.7	LO		1.7	—	
D84	FD	L	3.8	—		3.8	—		1.8	*LO*	
K85	FD	L	4.0	—		4.0	—		2.0	LO	

N86	FD	L	4.8	—		4.8	—		2.8	LO	
G87	FD	L	4.8	LO		4.8	LO		2.8	LO	
K88	FD	L	4.3	—		4.3	—		2.3	LO	
P89	FD	L		—[e]			—[e]			—[e]	
H90	FD	L	3.9	LO		3.9	LO		2.5	LO	
K91	FD	L	4.3	LO		4.3	LO		2.8	**-5.3**	**8.1**
V92	FD	L	3.6	LO		3.6	LO		1.6	—	
R93	FD	B4	4.1	-3.2	7.4	4.1	-2.9	7.1	2.1	-4.4	6.5
L94	FD	B4	3.8	LO		3.8	-2.0	5.9	1.8	-2.4	4.2
Y95	FD	B4	3.7	**-5.7**	**9.4**	3.7	**-5.7**	**9.4**	1.7	**-5.3**	**7.0**
[II]S96	FD	B4	4.6	**-5.7**	**10**	4.6	-5.0	9.6	2.6	**-5.3**	**7.9**
[I]I97	FD	L	3.8	—		3.8	—		1.8	—	
[II]A98	FD	L	4.0	-5.0	8.9	4.0	**-5.7**	**9.7**	2.0	LO	
S99	FD	L	4.6	-5.0	9.5	4.6	-4.6	9.1	2.6	**-5.3**	**7.9**
S100	FD	L	4.9	-2.0	6.8	4.9	-1.2	6.0	2.9	-3.0	5.8
A101	FD	L	4.5	LO		4.5	LO		2.5	-1.9	4.4
I102	FD	L	3.5	LO		3.5	LO		1.5	-1.9	3.4
G103	FD	L	4.2	-2.7	7.0	4.2	-2.4	6.7	2.2	-3.9	6.1
D104	FD	L	4.1	-0.7	4.8	4.1	LO		2.1	-2.0	4.0
F105	FD	L	3.8	LO		3.8	LO		1.8	-1.9	3.7
G106	FD	L	4.5	LO		4.5	LO		2.5	-1.5	4.1
D107	FD	L	4.1	LO		4.1	LO		2.1	-1.5	3.6
S108	FD	L	4.4	-0.6	5.0	4.4	LO		2.4	-2.5	4.9
K109	FD	L	4.5	LO		4.5	LO		2.5	-2.0	4.4
T110	FD	B5	4.2	-1.5	5.8	4.2	-1.2	5.4	2.2	-3.2	5.4
[I]V111	FD	B5	3.7	-6.0	9.7	3.7	-4.7	8.4	1.7	**-5.3**	**7.0**
S112	FD	B5	4.4	—[e]		4.4	—[e]		2.4	—[e]	
[I]L113	FD	B5	3.9	—[e]		3.9	—[e]		1.9	*-5.1*	*7.0*
[II]C114	FD	B5	4.5	—[e]		4.5	—[e]		2.5	—[e]	
[I]V115	FD	B5	4.0	**-5.7**	**9.6**	4.0	**-5.7**	**9.6**	2.0	**-5.3**	**7.3**
K116	FD	B5	4.0	-4.9	8.9	4.0	-3.5	7.5	2.0	—	
R117	FD	L	4.4	-1.6	5.9	4.4	LO		2.4	-3.6	6.0

Residue											
L118	FD	L	3.8	-2.5	6.3	3.8	-2.4	6.3	1.8	-4.3	6.1
I119	FD	B5-1	3.3	LO		3.3	LO		1.3	—	
Y120	FD	B5-1	3.7	-1.7	5.4	3.7	-1.1	4.8	1.7	LO	
T121	FD	B5-1	4.2	LO		4.2	LO		2.2	—	
N122	FD	L	4.9	LO		4.9	LO		2.9	-1.0	3.9
D123	FD	L	4.2	—		4.2	—		2.2	LO	
A124	FD	L	4.0	LO		4.0	LO		2.0	LO	
G125	FD	L	4.5	LO		4.5	LO		2.5	LO	
E126	FD	L	3.9	LO		3.9	LO		1.9	LO	
I127	FD	B5-2	3.3	LO		3.3	LO		1.3	*-5.3*	*6.6*
V128	FD	B5-2	3.3	-1.4	4.7	3.3	-1.2	4.5	1.3	-3.2	4.5
K129	FD	B5-2	4.0	LO		4.0	LO		2.0	LO	
G130	FD	L	4.6	-2.3	6.8	4.6	-2.0	6.6	2.6	-3.7	6.3
V131	FD	A1	3.7	-0.7	4.3	3.7	LO		1.7	-2.4	4.1
[I]C132	FD	A1	4.6	-1.7	6.3	4.6	-1.2	5.8	2.6	-2.9	5.5
S133	FD	A1	5.0	-3.3	8.3	5.0	-3.1	8.1	3.0	*-4.8*	*7.8*
N134	FD	A1	5.0	—[e]		5.0	—[e]		3.0	—[e]	
F135	FD	A1	4.3	—		4.3	—		2.3	LO	
[I]L136	FD	A1	3.7	—		3.7	—		1.7	—	
[I]C137	FD	A1	4.5	**-5.7**	**10**	4.5	**-5.7**	**10**	2.5	*-5.3*	*7.9*
D138	FD	L	4.4	**-5.0**	**9.3**	4.4	**-5.7**	**10**	2.4	-5.5	7.9
L139	FD	L	3.4	**-5.7**	**9.1**	3.4	**-5.7**	**9.1**	1.4	**-5.3**	**6.8**
Q140	FD	L	4.0	-3.4	7.5	4.0	-3.6	7.6	2.0	-3.1	5.1
P141	FD	L		—[e]			—[e]			—[e]	
G142	FD	L	4.2	-2.3	6.5	4.2	-1.1	5.4	2.2	—	
D143	FD	L	4.1	-3.3	7.4	4.1	-3.3	7.4	2.1	-4.8	6.9
N144	FD	B6	4.5	LO		4.5	LO		2.5	LO	
[I]V145	FD	B6	3.8	**-5.7**	**9.5**	3.8	-6.1	9.9	1.8	*-5.3*	*7.1*
Q146	FD	B6	4.1	-2.8	7.0	4.1	-2.7	6.8	2.1	-4.2	6.3
[I]I147	FD	B6	3.7	—		3.7	—		1.7	**-5.3**	**7.0**
T148	FD	B6	3.9	**-5.7**	**9.6**	3.9	-4.2	8.0	1.9	-3.8	5.6
G149	FD	B6	4.7	LO		4.7	LO		2.7	-1.9	4.5

[I]P150	FD	B6		—[e]			—[e]			—[e]	
V151	FD	B6	3.3	-1.9	5.2	3.3	LO		1.3	-3.3	4.5
G152	FD	L	4.3	—		4.3	—		2.3	LO	
K153	FD	L	4.3	LO		4.3	-1.3	5.6	2.3	LO	
E154	NRD	L	3.8	—		3.8	—		1.8	LO	
[II]M155	NRD	L	4.0	—		4.0	—		2.0	LO	
[I]L156	NRD	L	3.7	-2.0	5.7	3.7	-1.1	4.9	1.7	-3.1	4.9
[II]M157	NRD	L	4.0	-0.7	4.7	4.0	LO		2.0	-2.5	4.4
[II]P158	NRD	L		—[e]			—[e]			—[e]	
K159	NRD	L	3.9	—		3.9	LO		1.9	—	
D160	NRD	L	4.0	—		4.0	LO		2.0	LO	
P161	NRD	L		—[e]			—[e]			—[e]	
N162	NRD	L	4.4	LO		4.4	LO		2.4	-1.8	4.2
[II]A163	NRD	L	4.5	-3.1	7.6	4.5	-2.9	7.4	2.5	-4.6	7.1
T164	NRD	B1	4.1	-4.8	8.9	4.1	-4.0	8.1	2.1	**-5.3**	**7.4**
[II]I165	NRD	B1	3.7	**-5.7**	**9.4**	3.7	-4.8	8.5	1.7	**-5.3**	**7.0**
[III]I166	NRD	B1	3.2	**-5.7**	**8.9**	3.2	-4.8	8.0	1.2	**-5.3**	**6.6**
[II]M167	NRD	B1	4.0	**-5.7**	**9.6**	4.0	-4.6	8.5	2.0	**-5.3**	**7.3**
[III]L168	NRD	B1	3.7	**-5.7**	**9.4**	3.7	-4.6	8.3	1.7	**-5.3**	**7.0**
A169	NRD	B1	4.0	**-5.7**	**9.7**	4.0	-4.8	8.8	2.0	**-5.3**	**7.3**
T170	NRD	B1	4.1	-2.9	7.0	4.1	-2.7	6.9	2.1	-4.7	6.9
G171	NRD	A1	4.7	LO		4.7	LO		2.7	LO	
T172	NRD	A1	4.3	LO		4.3	LO		2.3	LO	
G173	NRD	A1	4.7	-1.9	6.5	4.7	-1.7	6.4	2.7	**-5.3**	**8.0**
[II]I174	NRD	A1	3.6	—		3.6	—		1.6	**-5.3**	**7.0**
[II]A175	NRD	A1	4.0	-4.4	8.4	4.0	-4.4	8.4	2.0	**-5.3**	**7.3**
[II]P176	NRD	A1		—[e]			—[e]			—[e]	
[II]F177	NRD	A1	3.7	-4.6	8.3	3.7	-4.6	8.3	1.7	**-5.3**	**7.0**
R178	NRD	A1	4.3	**-5.7**	**10**	4.3	-4.7	9.0	2.3	**-5.3**	**7.7**
S179	NRD	A1	4.8	-4.1	8.9	4.8	-4.2	9.0	2.8	**-5.3**	**8.1**
[II]F180	NRD	A1	4.3	***-4.3***	***8.5***	4.3	-4.7	8.9	2.3	**-5.3**	**7.6**
[II]L181	NRD	A1	3.7	**-5.7**	**9.4**	3.7	-4.5	8.2	1.7	***-5.3***	***7.0***

W182	NRD	A1	3.6	—[e]		3.6	—[e]		1.6	—[e]	
K183	NRD	A1	4.0	*-4.3*	*8.4*	4.0	*-3.9*	*8.0*	2.0	—	
[II]M184	NRD	A1	4.3	**-5.7**	***10***	4.3	**-5.7**	**10**	2.3	**-5.3**	**7.6**
[II]F185	NRD	L	4.1	**-5.7**	**9.8**	4.1	-4.2	8.3	2.1	**-5.3**	**7.4**
F186	NRD	L	4.0	-1.6	5.6	4.0	LO		2.0	-3.0	5.0
E187	NRD	L	3.7	—		3.7	—		1.8	—	
K188	NRD	L	4.0	—		4	—		2.0	—	
H189	NRD	L	4.2	—		4.2	—		2.8	—	
D190	NRD	L	4.0	—[e]		4.0	—[e]		2.5	—[e]	
D191	NRD	L	3.7	—		3.7	—		1.7	—	
Y192	NRD	L	3.7	LO		3.7	LO		1.8	LO	
K193	NRD	L	4.2	LO		4.2	LO		2.2	LO	
[II]F194	NRD	L	4.1	LO		4.1	LO		2.1	LO	
N195	NRD	L	4.7	LO		4.7	LO		2.7	LO	
G196	NRD	L	4.8	—		4.8	—		2.8	LO	
L197	NRD	B2	3.8	-3.1	6.9	3.8	-3.0	6.8	1.8	-4.5	6.3
[II]G198	NRD	B2	4.3	**-5.7**	**9.9**	4.3	-4.7	8.9	2.3	**-5.3**	**7.6**
[III]W199	NRD	B2	4.0	-5.0	8.9	4.0	-4.6	8.5	2.0	**-5.3**	**7.3**
[II]L200	NRD	B2	3.5	**-5.7**	**9.2**	3.5	-4.6	8.1	1.5	**-5.3**	**6.8**
[III]F201	NRD	B2	3.7	**-5.7**	**9.4**	3.7	-6.2	9.9	1.7	**-5.3**	**7.1**
[II]L202	NRD	B2	3.7	—		3.7	—		1.7	—	
G203	NRD	B2	4.3	LO		4.3	LO		2.3	—	
[II]V204	NRD	B2	3.7	-1.7	5.4	3.7	-1.0	4.7	1.7	-3.5	5.1
P205	NRD	L		—[e]			—[e]			—[e]	
T206	NRD	L	3.9	LO		3.9	LO		1.9	—	
S207	NRD	A2-1	4.8	LO		4.8	LO		2.8	LO	
S208	NRD	A2-1	4.9	—[e]		4.9	—[e]		2.9	—[e]	
S209	NRD	A2-1	4.9	LO		4.9	LO		2.9	-1.3	4.1
[II]L210	NRD	L	3.9	LO		3.9	LO		1.9	LO	
[II]L211	NRD	L	3.4	—[e]		3.4	—[e]		1.4	—[e]	
Y212	NRD	L	3.7	LO		3.7	LO		1.7	-1.4	3.1
K213	NRD	A2	4.2	—		4.2	LO		2.2	—	

Residue	Domain	Element	1			2			3		
E214	NRD	A2	3.8	—		3.8	—		1.8	LO	
E215	NRD	A2	3.5	LO		3.5	LO		1.6	LO	
[II]F216	NRD	A2	3.8	—		3.8	—		1.8	-5.1	6.9
G217	NRD	A2	4.5	LO		4.5	LO		2.5	—	
K218	NRD	A2	4.3	LO		4.3	LO		2.3	-1.1	3.4
[II]M219	NRD	A2	4.3	-1.4	5.7	4.3	-2.1	6.4	2.3	*LO*	
K220	NRD	A2	4.3	LO		4.3	LO		2.3	-2.2	4.4
E221	NRD	A2	3.8	LO		3.8	LO		1.8	-2.0	3.8
R222	NRD	A2	4.1	LO		4.1	LO		2.1	-1.5	3.6
A223	NRD	L	4.4	LO		4.4	LO		2.4	-2.0	4.4
P224	NRD	L		—[e]			—[e]			—[e]	
E225	NRD	L	3.4	LO		3.4	LO		1.5	—	
N226	NRD	L	4.5	LO		4.5	LO		2.5	LO	
[II]F227	NRD	B3	4.3	-1.3	5.6	4.3	-0.9	5.2	2.3	-2.9	5.2
R228	NRD	B3	4.3	—		4.3	—		2.3	**-5.3**	**7.7**
[II]V229	NRD	B3	3.7	LO		3.7	LO		1.7	-0.7	2.4
D230	NRD	B3	3.8	-2.7	6.4	3.8	-2.7	6.4	1.8	-4.2	5.9
Y231	NRD	B3	3.7	LO		3.7	LO		1.8	LO	
A232	NRD	B3	4.2	-1.0	5.3	4.2	LO		2.2	-3.3	5.5
[II]V233	NRD	B3	3.5	—		3.5	—		1.5	LO	
S234	NRD	L	4.4	LO		4.4	LO		2.4	—	
R235	NRD	L	4.6	LO		4.6	LO		2.6	LO	
E236	NRD	L	3.9	LO		3.9	LO		1.9	LO	
Q237	NRD	L	4.1	LO		4.1	LO		2.1	LO	
T238	NRD	L	4.3	LO		4.3	LO		2.3	LO	
N239	NRD	L	4.9	LO		4.9	LO		2.9	LO	
A240	NRD	L	4.5	—[e]		4.5	—[e]		2.5	—[e]	
A241	NFD	L	4.2	LO		4.2	LO		2.2	—	
G242	NFD	L	4.5	LO		4.5	LO		2.5	LO	
E243	NFD	L	3.9	LO		3.9	LO		1.9	LO	
R244	NFD	L	4.1	LO		4.1	LO		2.1	LO	
M245	NFD	L	4.4	LO		4.4	LO		2.4	LO	

Y246	NFD	L	4.0	LO		4.0	LO		2.0	LO	
[III]I247	NFD	A3	3.5	—		3.5	—		1.5	LO	
Q248	NFD	A3	4.0	LO		4.0	LO		2.0	-0.7	2.7
T249	NFD	A3	4.3	LO		4.3	LO		2.3	LO	
R250	NFD	A3	4.5	LO		4.5	LO		2.5	-1.4	3.9
[III]M251	NFD	A3	4.4	LO		4.4	LO		2.4	-2.4	4.8
A252	NFD	A3	4.3	—		4.3	—		2.3	-2.2	4.6
E253	NFD	L	3.7	LO		3.7	LO		1.7	-1.3	3.0
Y254	NFD	L	3.8	—		3.8	—		1.8	-2.9	4.6
K255	NFD	A4	4.2	LO		4.2	LO		2.2	-1.1	3.3
E256	NFD	A4	3.8	LO		3.8	LO		1.8	*LO*	
E257	NFD	A4	3.5	LO		3.5	LO		1.6	LO	
[III]L258	NFD	A4	3.5	-2.7	6.2	3.5	-2.6	6.1	1.5	-4.2	5.6
[III]W259	NFD	A4	3.6	-1.9	5.4	3.6	-1.9	5.4	1.6	-3.3	4.9
E260	NFD	L	3.6	-1.9	5.5	3.6	-1.9	5.4	1.6	-3.4	5.0
L261	NFD	L	3.5	-3.1	6.6	3.5	-3.1	6.5	1.5	-5.3	6.7
[III]L262	NFD	L	3.4	-4.6	8.0	3.4	*-4.1*	*7.5*	1.4	—	
K263	NFD	L	3.9	LO		3.9	LO		1.9	-2.1	4.1
K264	NFD	L	4.3	—		4.3	LO		2.3	—	
D265	NFD	L	4.0	—		4.0	—		2.0	—	
N266	NFD	L	4.5	LO		4.5	LO		2.5	LO	
[III]T267	NFD	B4	4.4	-2.7	7.1	4.4	-2.6	7.0	2.4	-3.9	6.4
Y268	NFD	B4	4.1	**-5.7**	**9.8**	4.1	-4.7	8.8	2.1	**-5.3**	**7.4**
[III]V269	NFD	B4	3.5	**-5.7**	**9.2**	3.5	-4.3	7.9	1.5	**-5.3**	**6.9**
[II]Y270	NFD	B4	3.8	**-5.7**	**9.5**	3.8	-4.7	8.5	1.8	**-5.3**	**7.1**
[III]M271	NFD	B4	4.2	**-5.7**	**9.9**	4.2	-4.4	8.6	2.2	—	
[II]C272	NFD	B4	4.9	**-5.7**	**11**	4.9	-4.5	9.4	2.9	**-5.3**	**8.2**
G273	NFD	B4	4.9	-1.8	6.7	4.9	-1.1	6.1	2.9	-3.5	6.4
L274	NFD	B4	3.8	—		3.8	—		1.8	-2.3	4.1
K275	NFD	L	3.9	LO		3.9	—		1.9	—	
G276	NFD	L	4.6	—[e]		4.6	—[e]		2.6	—[e]	
[III]M277	NFD	A5	4.4	—[e]		4.4	—[e]		2.4	—[e]	

E278	NFD	A5	3.8	—[e]		3.8	—[e]		1.8	—[e]
K279	NFD	A5	4.0	LO		4.0	LO		2.0	—
G280	NFD	A5	4.6	LO		4.6	LO		2.6	—
[III]I281	NFD	A5	3.6	LO		3.6	LO		1.6	LO
D282	NFD	A5	3.7	LO		3.7	LO		1.7	—
D283	NFD	A5	3.7	LO		3.7	LO		1.7	-1.4	3.2
I284	NFD	A5	3.3	-0.7	4.0	3.3	LO		1.3	-2.6	3.9
[III]M285	NFD	A5	4.0	-3.0	7.0	4.0	-2.9	6.9	2.0	—
V286	NFD	A5	3.6	-2.1	5.7	3.6	-2.2	5.8	1.6	-3.7	5.3
S287	NFD	A5	4.4	LO		4.4	LO		2.4	—
L288	NFD	A5	3.9	LO		3.9	LO		1.9	-1.1	3.0
[III]A289	NFD	A5	4.0	LO		4.0	LO		2.0	—
E290	NFD	L	3.7	LO		3.7	LO		1.7	-1.9	3.6
K291	NFD	L	4.0	LO		4.0	LO		2.0	—
D292	NFD	L	4.0	LO		4.0	LO		2.0	-1.2	3.2
G293	NFD	L	4.3	LO		4.3	LO		2.3	LO
I294	NFD	L	3.6	-1.2	4.8	3.6	LO		1.6	-2.7	4.4
D295	NFD	L	3.7	LO		3.7	LO		1.7	—
[III]W296	NFD	A6	3.6	LO		3.6	LO		1.6	LO
F297	NFD	A6	3.8	LO		3.8	LO		1.8	-0.7	2.6
D298	NFD	A6	4.0	**-5.7**	**9.6**	4.0	**-5.7**	**9.6**	2.0	—
Y299	NFD	A6	3.7	-1.5	5.2	3.7	-1.2	4.9	1.8	-2.9	4.7
K300	NFD	A6	4.2	-2.6	6.8	4.2	-2.3	6.5	2.2	-4.2	6.4
K301	NFD	A6	4.3	-0.7	4.9	4.3	LO		2.3	-2.5	4.8
Q302	NFD	A6	4.4	LO		4.4	LO		2.4	-1.2	3.6
L303	NFD	A6	3.8	LO		3.8	LO		1.8	—
K304	NFD	A6	3.9	—		3.9	—		1.9	—
R305	NFD	A6	4.4	LO		4.4	LO		2.4	-1.2	3.6
G306	NFD	A6	4.7	LO		4.7	LO		2.7	-1.5	4.2
D307	NFD	L	4.1	LO		4.1	LO		2.1	LO
Q308	NFD	L	4.1	-1.4	5.5	4.1	-1.0	5.1	2.1	-2.8	4.9
[III]W309	NFD	B5	4.0	-1.7	5.7	4.0	-1.2	5.2	2.0	-3.3	5.3

[II]N310	NFD	B5	4.6	-3.8	8.4	4.6	-3.3	7.8	2.6	—
V311	NFD	B5	3.8	LO		3.8	LO		1.8	—
E312	NFD	B5	3.5	-3.4	7.0	3.5	-2.8	6.4	1.6	-4.9	6.4
[III]V313	NFD	B5	3.3	-0.6	4.0	3.3	LO		1.4	-1.7	3.1
Y314	NFD	B5	2.0	-2.8	4.8	2.0	-2.7	4.7	0.0	-3.4	3.4